Tubulin transport by IFT is upregulated during ciliary growth by a cilium-autonomous mechanism

Julie M. Craft,[1] J. Aaron Harris,[1] Sebastian Hyman,[1] Peter Kner,[2] and Karl F. Lechtreck[1]

[1]Department of Cellular Biology and [2]College of Engineering, University of Georgia, Athens, GA 30602

The assembly of the axoneme, the structural scaffold of cilia and flagella, requires translocation of a vast quantity of tubulin into the growing cilium, but the mechanisms that regulate the targeting, quantity, and timing of tubulin transport are largely unknown. In *Chlamydomonas*, GFP-tagged α-tubulin enters cilia as an intraflagellar transport (IFT) cargo and by diffusion. IFT-based transport of GFP-tubulin is elevated in growing cilia and IFT trains carry more tubulin. Cells possessing both nongrowing and growing cilia selectively target GFP-tubulin into the latter. The preferential delivery of tubulin boosts the concentration of soluble tubulin in the matrix of growing versus steady-state cilia. Cilia length mutants show abnormal kinetics of tubulin transport. We propose that cells regulate the extent of occupancy of IFT trains by tubulin cargoes. During ciliary growth, IFT concentrates soluble tubulin in cilia and thereby promotes elongation of the axonemal microtubules.

Introduction

Microtubules, polymers of α- and β-tubulin dimers, are the major structural element of motile and nonmotile cilia and flagella (Borisy and Taylor, 1967). Microtubules form the scaffold onto which other axonemal structures such as dynein arms and radial spokes are attached; they also serve as tracks for intraflagellar transport (IFT), a bidirectional motility which is required for ciliary assembly (Kozminski et al., 1993, 1995). During ciliary growth, large amounts of tubulin dimers need to be transported into the organelle. Like cytoplasmic microtubules, the axonemal microtubules grow through the addition of tubulin subunits to the distal plus-ends (Witman, 1975; Euteneuer and McIntosh, 1981; Johnson and Rosenbaum, 1992). Thus, the delivery of tubulin into cilia and its translocation to the ciliary tip are prerequisites for ciliary assembly.

Several lines of evidence suggest that inside cilia, tubulin is transported by IFT. In the conditional *Chlamydomonas fla10-1* mutant, the incorporation of epitope-tagged tubulin at the distal end of cilia is decreased after a shutdown of IFT (Marshall and Rosenbaum, 2001). In vitro, tubulin dimers directly interact with a tubulin-binding module formed by the IFT particle proteins IFT74 and IFT81 (Bhogaraju et al., 2013). Expression of fluorescent tubulin in *Caenorhabditis elegans* revealed weak tracks, possibly representing tubulin transport in sensory cilia, and FRAP analysis supported the notion that tubulin transport is IFT-dependent (Hao et al., 2011). It remains largely unknown how tubulin transport is coordinated with ciliary growth. Insufficient delivery of tubulin could result in slower growth and shorter cilia, whereas an excess of tubulin might promote the assembly of excessively long cilia. Defects in ciliary length impair the motile and sensory functions of cilia and have been linked to ciliary diseases (Mahjoub et al., 2005; Tammachote et al., 2009; Ko et al., 2010; Özgül et al., 2011; Mahjoub and Stearns, 2012; Tam et al., 2013).

In the unicellular alga *Chlamydomonas reinhardtii*, IFT and protein transport inside cilia can be imaged with single particle sensitivity using total internal reflection fluorescence (TIRF) microscopy (Lechtreck, 2013; Wren et al., 2013). Recently, stable expression of a fluorescent protein-tagged α-tubulin was accomplished in *C. reinhardtii* (Rasala et al., 2013). Ciliogenesis can be experimentally induced by removing the existing cilia (Rosenbaum et al., 1969), allowing for an in-depth study of the relationship between tubulin transport and ciliary growth using direct imaging. A genetic analysis of the regulation of tubulin transport is aided by numerous *C. reinhardtii* mutants with defects in ciliary assembly and length control.

Here, using two-color imaging, we show that GFP–α-tubulin is primarily transported by IFT but some GFP-tubulin also

Correspondence to Karl Lechtreck: lechtrek@uga.edu

Abbreviations used in this paper: CHX, cycloheximide; IFT, intraflagellar transport; MM fraction, membrane+matrix fraction; TZ, transition zone.

The Rockefeller University Press $30.00
J. Cell Biol. Vol. 208 No. 2 223–237
www.jcb.org/cgi/doi/10.1083/jcb.201409036

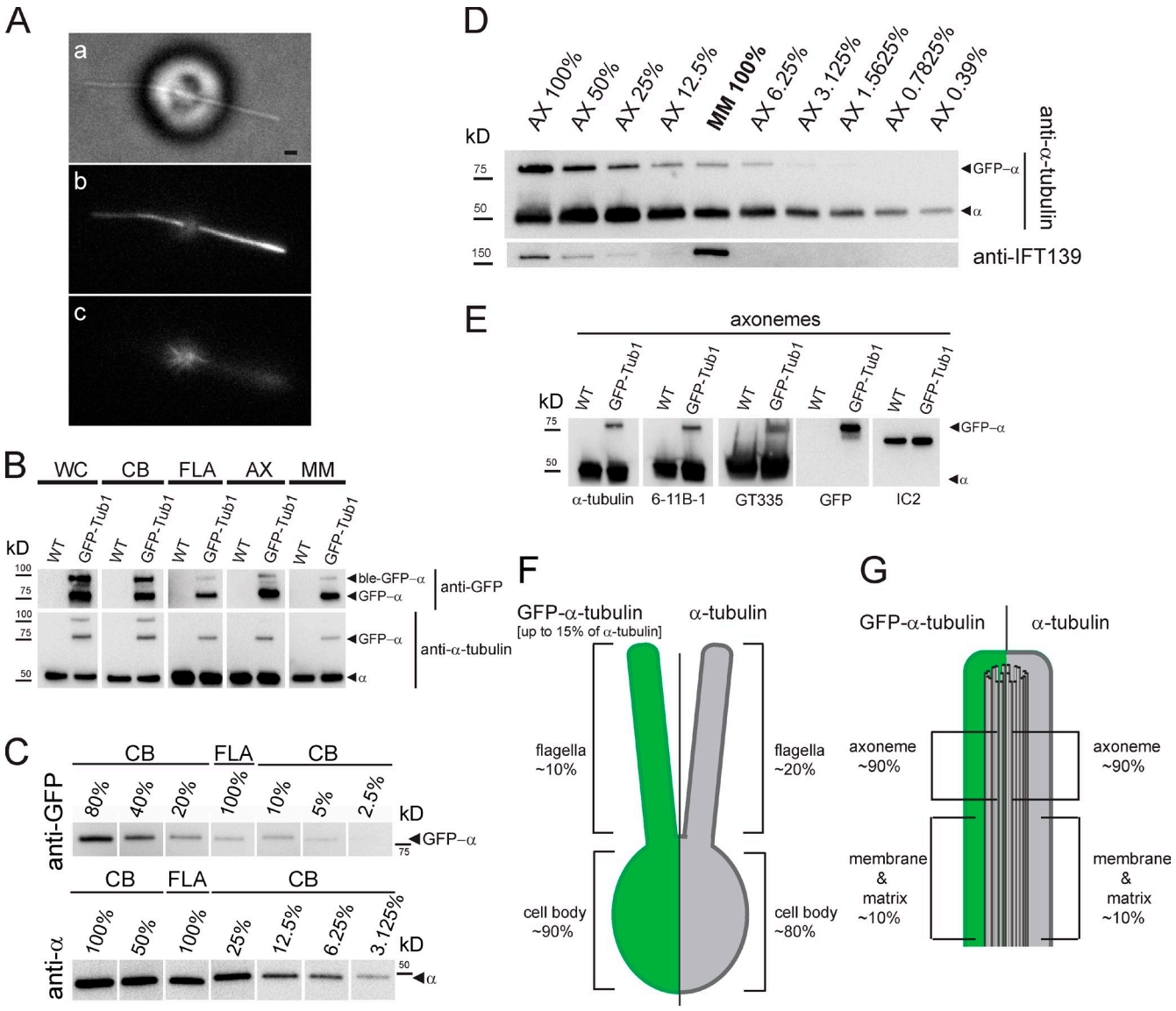

Figure 1. **GFP-tagged and endogenous α-tubulin have similar properties.** (A) Bright-field (a) and TIRF (b and c) images of a live cell expressing GFP–α-tubulin. The two focal planes show cilia (b) and cell body microtubules (c). Bar, 1 µm. (B) Western blot analysis of wild type (WT) and the GFP–α-tubulin expressing strain GFP-Tub1. Whole cells (WC), cell bodies (CB), isolated cilia (FLA), axonemes (AX), and MM fractions were loaded and probed with antibodies to GFP and α-tubulin. The bands corresponding to α-tubulin, GFP–α-tubulin, and the uncleaved ble-GFP–α-tubulin are marked. (C) Western blots probed with anti–α-tubulin and anti-GFP showing different dilutions of the cell body (CB) sample in comparison to the undiluted cilia sample (FLA). The amounts of endogenous and tagged tubulin in cilia correspond to ∼20 and ∼10% of the respective cell body tubulin. (D) Western blot showing a dilution series of axonemes (AX) and undiluted MM of strain GFP-Tub1 to determine the distribution of tagged and endogenous tubulin inside cilia. The blot was probed with antibodies to α-tubulin and the matrix protein IFT139. (E) Western blots of wild-type and GFP-Tub1 axonemes probed with antibodies to α-tubulin, acetylated α-tubulin (6-11B-1), polyglutamylated tubulin (GT335), GFP, and, as a loading control, IC2, an outer arm dynein intermediate chain. (F and G) Schematic presentations of the distribution of GFP-tagged tubulin and endogenous tubulin in whole cells (F) and cilia (G).

enters cilia by diffusion. The frequency of tubulin transport events by anterograde IFT was greatly increased during ciliary growth. We find that *C. reinhardtii* cells possess the ability to preferentially direct IFT-bound tubulin into growing cilia, indicating that tubulin transport is regulated in a cilium-autonomous manner. Dysregulation of tubulin transport was observed in the cilia length mutants *short flagella2* and *long flagella2-1*, indicating a possible link between the ciliary length regulation and tubulin transport by IFT. During ciliary growth, the concentration of soluble tubulin in the ciliary matrix was elevated substantially above that of steady-state cilia. We propose a model in which cells use IFT to regulate the concentration of soluble tubulin inside cilia; a high concentration of tubulin in the matrix will promote microtubule polymerization and ciliary growth.

Results

Endogenous and GFP-tagged α-tubulin show a similar distribution

To express GFP–α-tubulin in *C. reinhardtii* for imaging in vivo, we used the recently described fusion construct consisting of the zeocin resistance gene *BLE* and the *TUA2* gene separated

by the viral 2A sequence encoding a self-cleaving peptide and replaced the original mCerulean with the brighter superfolder GFP (hereafter referred to as GFP; Rasala et al., 2013). In vivo microscopy revealed the presence of GFP–α-tubulin in cilia and cell body microtubules (Fig. 1 A; Rasala et al., 2013). Western blotting of whole cells with anti-GFP identified a major ∼78 kD and a minor ∼104 kD band that were both also recognized by anti–α-tubulin (Fig. 1 B). The former represents GFP–α-tubulin; the latter, largely excluded from cilia (Fig. 1 B), is the uncleaved ble-GFP–α-tubulin fusion protein. The expression levels of GFP–α-tubulin varied between individual transformants. In the strain GFP-Tub1, which was used in most experiments, GFP–α-tubulin amounted to ∼15% of the endogenous α-tubulin (Fig. 1 B). To determine the distribution of GFP-tagged and endogenous α-tubulin, cells were fractionated and analyzed by Western blotting (Fig. 1, B–D). Staining with anti–α-tubulin revealed that ∼80% of endogenous tubulin resides in the cell body and ∼20% enters the cilia; a similar partition was observed for GFP–α-tubulin with ∼90% in the cell body and ∼10% in cilia (Fig. 1, C and F). Inside steady-state cilia, both tagged and endogenous tubulin showed a similar distribution with ∼90% incorporated into the axoneme and <10% remaining soluble in the membrane+matrix fraction (MM fraction; Fig. 1, D and G). Immunoprecipitation using anti-GFP beads revealed that GFP–α-tubulin forms a complex with endogenous β-tubulin in the ciliary matrix (Fig. S1, A and B). Axonemal tubulin is known to undergo numerous posttranslational modifications (PTMs; Gaertig and Wloga, 2008). Western blots of fractionated cilia probed with PTM-specific antibodies showed that GFP–α-tubulin undergoes K40 acetylation and polyglutamylation, especially in the axoneme (Fig. 1 E and Fig. S1 C). In summary, GFP–α-tubulin behaves largely similar to the endogenous protein, validating its use as a reporter of tubulin transport.

Tubulin is a cargo of IFT

To image GFP–α-tubulin during transport, cilia were first photobleached to eliminate the signal resulting from the presence of GFP–α-tubulin in the axonemes and then analyzed by TIRF microscopy. Kymograms (time-space plots) showed individual GFP–α-tubulin particles diffusing inside cilia or undergoing active transport with constant velocities indicative for IFT (Fig. 2 A; Videos 1 and 2). Anterograde transport progressed at 1.68 µm/s (±0.21 µm/s; n = 1,404 particles) and occurred with a frequency of 0.3 particles/min in steady-state cilia (± 0.7 particles/min, n = 78 cilia); retrograde transport events were rarely observed and had a velocity of 3.05 µm/s (±1.1 µm/s, n = 35; Fig. 2 A, a and b). IFT moved the majority of GFP–α-tubulin particles directly from the ciliary base to the tip (98% of 1,281 particles; Fig. 2 B, a); transitions of GFP–α-tubulin from IFT to diffusion indicative of unloading along the ciliary shaft were observed as well (Fig. S2, C and D). To test directly if tubulin moves in association with IFT trains, GFP–α-tubulin was expressed in an *ift20-1* IFT20-mCherry strain (Fig. S3 B). Two-color imaging showed comigration of the tagged tubulin and IFT20-mCherry indicating that tubulin is a bona fide cargo of IFT (Fig. 2 B and Video 3).

Recent data revealed that the acidic C-terminal domain (E-hook) of β-tubulin but not that of α-tubulin is required for the in vitro interaction between tubulin dimers and IFT74–IFT81 complexes (Bhogaraju et al., 2013). We designed modified GFP–α-tubulins in which the E-hook was replaced with the corresponding region of β-tubulin, altered to substitute seven glutamate residues with alanine or glutamine, or removed entirely (Table S1). The altered α-tubulin molecules were expressed (as ∼5–15% of the endogenous α-tubulin; Fig. S3 A), transported by IFT, and incorporated into the axoneme (Table S1). Thus, our in vivo observations agree with the earlier in vitro study showing that the C-terminal E-hook of α-tubulin is dispensable for tubulin binding to IFT trains. The modified tubulins were expressed in the presence of endogenous wild-type tubulin indicating that *C. reinhardtii* tolerates some E-hook–deficient GFP–α-tubulins; a deletion of the E-hook from all of either α- or β-tubulin is lethal in *Tetrahymena* (Duan and Gorovsky, 2002).

Tubulin enters cilia by diffusion

To improve imaging of diffusing tubulin, photobleached cilia were observed at elevated laser intensities which quickly bleached most GFP preventing crowding of the cilia with fluorescent α-tubulin. For some experiments, superfolder GFP was replaced with the brighter mNeonGreen (Shaner et al., 2013). 64 individual GFP–α-tubulin particles were tracked while diffusing inside the ciliary shaft and the mean of the square displacement was determined in 30 subsequent frames (Fig. 2 C). This resulted in a 1D diffusion coefficient of 1.76 ± 0.18 µm^2/s for GFP–α-tubulin, a value similar to that determined for similarly sized soluble proteins diffusing in cilia (Lin et al., 2013). In agreement with this high mobility of GFP–α-tubulin, we observed "jumps" over almost the entire length of a cilium (Fig. 2 A, d; and Fig. S2, A, E, and I). In the vicinity of the ciliary tip, GFP-tagged tubulin mostly displayed a reduced mobility as reflected by a diffusion coefficient of ∼0.18 ± 0.02 µm^2/s (n = 58 trajectories; Fig. 2 A, d; Fig. S2, A, C, D, and F, white arrowheads; and Video 4). The reduced mobility of GFP-tubulin in the distal ∼0.5-µm ciliary segment could result, for example, from interactions with other proteins. Infrequently, GFP–α-tubulin diffusing near the tip of steady-state cilia was observed becoming stationary, which is indicative of incorporation into the axoneme (Fig. S2, F–H).

Although IFT-based transport of tubulin was rare in steady-state cilia, diffusing GFP-tubulin continuously entered fully photobleached cilia from the base (Fig. 2 A, c; Fig. S2 I; and Video 2). To test whether active IFT is required for the diffusional entry of tubulin into cilia, we expressed GFP–α-tubulin in the *C. reinhardtii fla10-1* mutant; IFT can be switched-off in this strain by incubating the cells at 32°C for several hours (Kozminski et al., 1995). IFT of GFP–α-tubulin was observed in *fla10-1* and wild-type steady-state cilia at the permissive temperature albeit at low frequencies (Fig. 2, D, a, and E). Cycloheximide (CHX) limits ciliary regeneration to half-length and we previously observed elevated transport of the axonemal protein DRC4 in such cilia (Wren et al., 2013). Similarly, an increased frequency of tubulin transport was observed in half-length cilia assembled by control or *fla10-1* in the presence of CHX at the permissive temperature (Fig. 2 E). After shifting such cells to 32°C for 180 min, IFT-like movements of GFP–α-tubulin were frequent in cilia of control cells but were not observed in the *fla10-1* cells; entry of

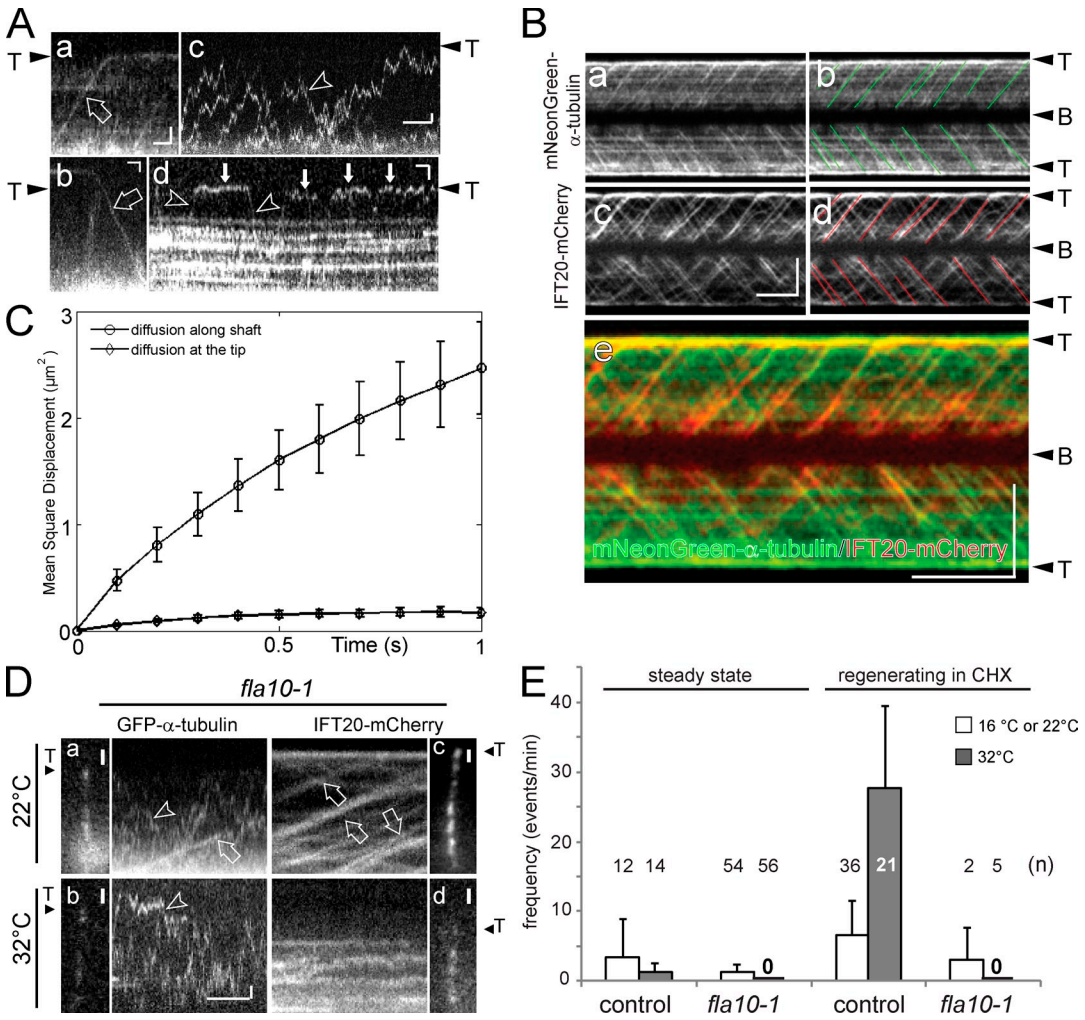

Figure 2. **Tubulin enters cilia by IFT and diffusion.** (A) Gallery of kymograms depicting GFP–α-tubulin (or, in c, mNeonGreen-tubulin) moving inside cilia by anterograde IFT (open arrow in a), retrograde IFT (open arrow in b), and diffusion (arrowheads in c and d). Anterograde transport results in trajectories running from the bottom left (ciliary base) to the top right (ciliary tip; T); retrograde transport events result in top-left to bottom-right trajectories. (c) Tubulin diffusing inside the ciliary shaft; (d) reduced mobility of GFP–α-tubulin in the vicinity of the tip (filled arrows). Bars, 1 µm and 1 s. (B) Kymograms from simultaneous imaging of mNeonGreen–α-tubulin (a and b) and IFT20-mCherry (c and d) in growing cilia; IFT-like trajectories are marked in b and d. A merged kymogram is shown in e. A Western blot of this strain is shown in Fig. S3 B. Bars, 5 µm and 5 s. (C) Mean square displacement versus time for 64 sfGFP–α-tubulin particles diffusing inside the shaft and 58 particles diffusing near the tip of steady-state cilia. The standard error of the mean at each value is indicated. A linear fit to the data at the short time points, which is likely to represent pure diffusion, results in diffusion coefficients of ∼1.8 $\mu m^2/s$ and ∼0.2 $\mu m^2/s$ for 1D diffusion of GFP-tubulin along the ciliary shaft and at the tip, respectively. (D) Still images and kymograms of *fla10-1* cells expressing either GFP–α-tubulin (a and b) or IFT20-mCherry (c and d) at the permissive temperature (22°C; a and c) and after >180 min at 32°C (b and d). IFT-like trajectories for tubulin and IFT20 were only observed at 22°C (open arrows in a and c). Diffusion of GFP–α-tubulin (arrowhead in b) into photobleached cilia continued at 32°C in the absence of detectable IFT (d). Bars, 1 µm and 1 s. (E) Frequency of anterograde GFP–α-tubulin transport by IFT in *fla10-1* and control cells (*FLA10 ift20-1* IFT20 mCherry). Steady-state cilia and cilia regenerated in the presence of CHX were compared; at 32°C, IFT-like tubulin transport was robust in control cells but not observed in *fla10-1* cells. *fla10-1* regenerates cilia only slowly at room temperature (∼22°C); most measurements are based on cells regenerating cilia at 16°C. Error bars indicate SEM.

GFP–α-tubulin by diffusion, however, continued (Fig. 2, D, b, and E). A strain expressing IFT20-mCherry in the *fla10-1 ift20-1* background was used to verify that IFT was indeed abolished at the conditions used (Fig. 2 D, c and d). The data indicate that GFP–α-tubulin enters cilia by diffusion.

The frequency of tubulin transport by IFT is regulated by the assembly status of cilia

To determine whether IFT transports more tubulin when cilia grow, we compared the transport frequencies of GFP–α-tubulin between steady-state and growing cilia. After amputation of cilia by a pH shock, cells regenerate full-length cilia within ∼90 min. Partially regenerated cilia were bleached and tubulin influx and incorporation into the cilia were analyzed (Fig. 3 A and Video 5). Fluorescent tubulin was rapidly added to the tip and the fluorescent distal parts of cilia lengthened, revealing that cilia continue to grow under TIRF illumination while immobilized in the observation chamber (Fig. 3 B). In growing cilia (∼3–10 µm in length), GFP–α-tubulin moved by anterograde IFT with a greatly elevated mean frequency of 18.3 ± 6.9 particles/min (n = 110 cilia) versus ∼0.3 particles/min observed in steady-state cilia of the same strain (Fig. 3 C). The transport frequency of GFP–α-tubulin remained elevated until cilia reached ∼10 µm in length and was then reduced to 1 ± 2.2 particles/min in cilia of 10–12 µm in

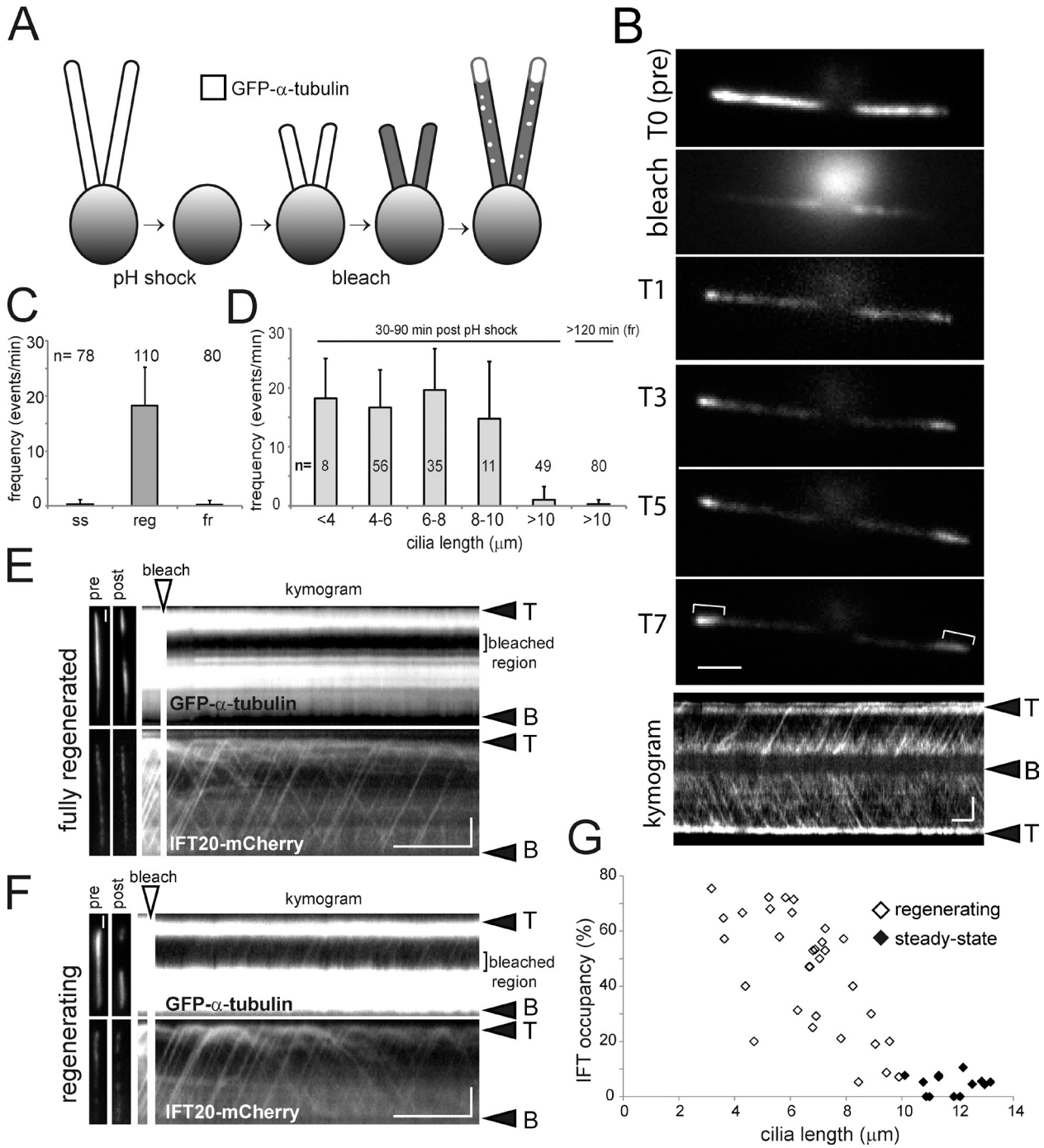

Figure 3. **IFT particles carry more tubulin during ciliary growth.** (A) Schematic presentation of the experimental design. Cells were deciliated by a pH shock and allowed to partially regrow cilia. Then, the cilia were bleached and the entry and assembly of unbleached GFP–α-tubulin was analyzed by TIRF. (B) Individual frames from videos captures before (T0), during (bleach), and at various time points (T1–T7 in min) after bleaching of the cilia. Brackets: unbleached GFP-tubulin added at the ciliary tip as cilia elongate. Bar, 2 µm. Bottom: kymogram of the same cell showing numerous IFT-like GFP-tubulin tracks. Bar, 2 µm and 2 s. (C) Mean frequency of GFP-tubulin transport by anterograde IFT in steady-state (ss), regenerating (reg), and fully regenerated (fr) cilia. Error bars indicate the standard deviation. (D) Analysis of GFP-tubulin transport frequency by anterograde IFT in regenerating cilia of various lengths. Error bars indicate SEM. (E and F) Segments of the cilia of cells coexpressing GFP–α-tubulin and IFT20-mCherry were bleached using a focused laser beam and protein traffic in the bleached region was analyzed by two-color TIRF microscopy. The kymogram of a cell with fully regrown flagella (E) shows numerous IFT20-mCherry trajectories, whereas transport of GFP–α-tubulin was not observed. In contrast, most IFT20-mCherry trajectories align with GFP–α-tubulin trajectories in the regenerating cilium (F). Bars, 2 µm and 5 s. (G) Scatter plot of the occupancy rate (the percentage of IFT20-mCherry particles moving together with GFP–α-tubulin) in cilia of different length. Cells with regenerating (white marks) or nongrowing (steady-state and fully regenerated, black marks) cilia were analyzed (n = 32 and 13 cilia, respectively).

length (n = 49 cilia) before returning to the pre-deciliation level (~0.3 ± 0.75 particles/min, n = 80 cilia at >2 h after pH shock; Fig. 3, C and D). The pattern indicates a strong length dependency of IFT-based tubulin transport and matches the deceleratory kinetics of cilia regeneration in *C. reinhardtii* with rapid elongation until cilia reach ~10 µm, followed by slower growth until

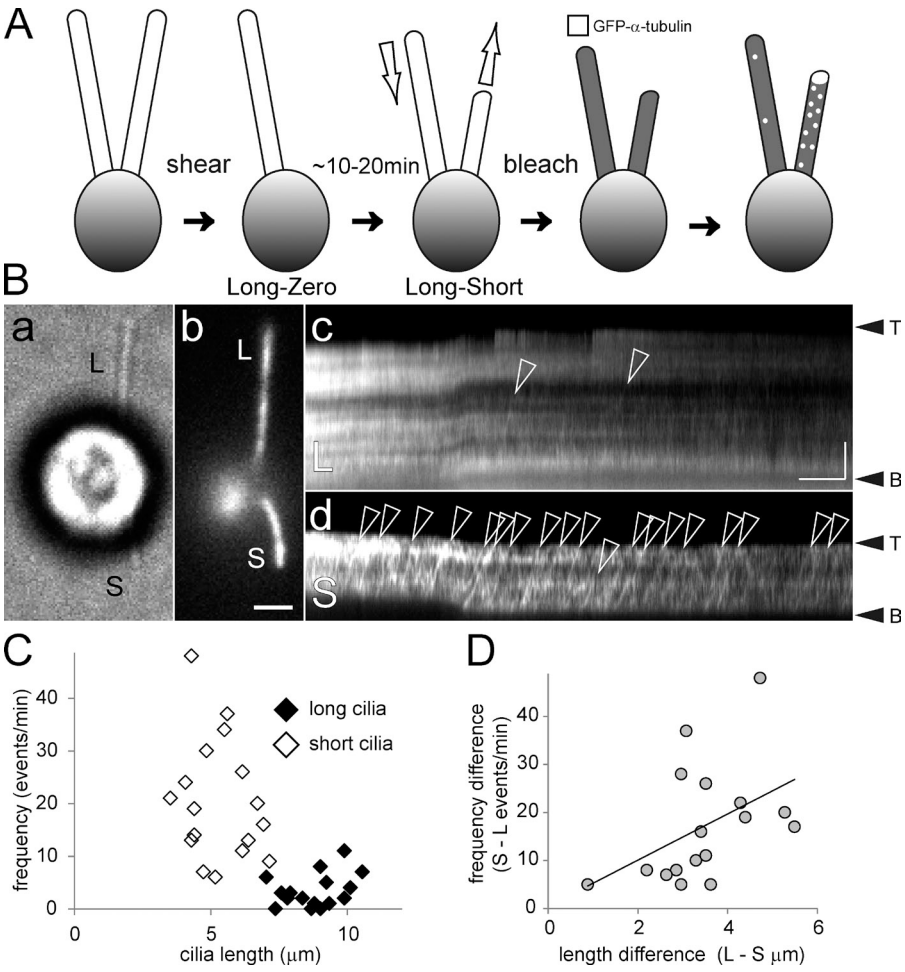

Figure 4. **Cilium-autonomous regulation of tubulin transport by IFT.** (A) Schematic presentation of the long-short experiment to generate cells with growing and nongrowing cilia. (B) Bright-field (a), TIRF image (b), and corresponding kymograms (c and d) of a long-short cell. Numerous GFP–α-tubulin transport events (open arrowheads) were observed in the short (S) cilium (d), whereas only a few such events were detected in the long (L) flagellum (c). Bars, 2 µm and 5 s (b and c). (C) Scatter plot of the frequencies of GFP–α-tubulin transport in short (open diamonds) and long (filled diamonds) cilia of long-short cells. (D) The difference in tubulin transport frequencies between the long and the short cilia of given cells diminished as the difference in length between the two cilia decreased (n = 17).

cilia reach their final length of ∼12 µm (Rosenbaum et al., 1969; Engel et al., 2009). In summary, tubulin transport by anterograde IFT is up-regulated during ciliary growth.

IFT particles carry more tubulin during ciliary growth

The observed increase in the transport of tubulin in growing cilia could be caused by an increase in the amount of tubulin carried by a given number of IFT trains or by an increase in the number of IFT trains without changing the tubulin load per train. In *C. reinhardtii*, similar amounts of IFT material are thought to be present in cilia regardless of their length (Marshall et al., 2005; Engel et al., 2009). Two-color imaging was used to determine the share of IFT particles participating in GFP-tubulin transport in regenerating and steady-state cilia (Fig. 3, E–G). Photobleaching of the entire cilia using increased 488-nm laser intensity also greatly diminished the signal from IFT20-mCherry making quantitative analyses unreliable. We therefore used a brief, focused laser beam in epifluorescence (∼3 µm diameter; ∼100–300 ms in duration) to bleach a ciliary segment and imaged the cilia in TIRF as particles reentered the bleached area (Fig. 3, E and F). IFT occupancy, i.e., the share of IFT20-mCherry–tagged anterograde IFT trains carrying GFP–α-tubulin, decreased from ∼80% during the initial rapid growth to ∼10% as cilia approached full length and even lower rates in fully regenerated and steady-state cilia (means were 45 ± 21% vs. 4.5 ± 3.5%, respectively; $P = 2.2 \times 10^{-8}$; Fig. 3 G). As previously shown, the IFT frequency was largely independent of ciliary length (Fig. S4 A; Dentler, 2005; Engel et al., 2009). In conclusion, IFT trains in regenerating cilia carry a larger load of tubulin than those in nongrowing cilia.

IFT transport of tubulin is regulated in a cilium-autonomous manner

How do cells regulate the loading of cargo onto IFT particles? To begin addressing this question, we tested whether tubulin transport is regulated at the cilium or cell level. After shearing of just one of the two cilia, cells will partially resorb the remaining cilium while regrowing the missing one giving so-called long-short cells (Fig. 4 A and see Fig. 6 E; Rosenbaum et al., 1969). An elevated tubulin transport in both cilia of a long-short cell would indicate a cell-wide regulation, whereas an increase limited to the growing cilium would indicate a regulation that operates at the single cilium level. The mean GFP–α-tubulin IFT frequencies were 20.5 particles/min for the short and 3.3 particles/min for the long cilia of long-short cells (n = 17; ±11.6 and 3.2 particles/min, respectively; Fig. 4, B and C; Video 6). In all long-short cells analyzed, the transport frequency in the short cilium exceeded that of the long one; this difference decreased as both cilia approached a similar length (Fig. 4 D).

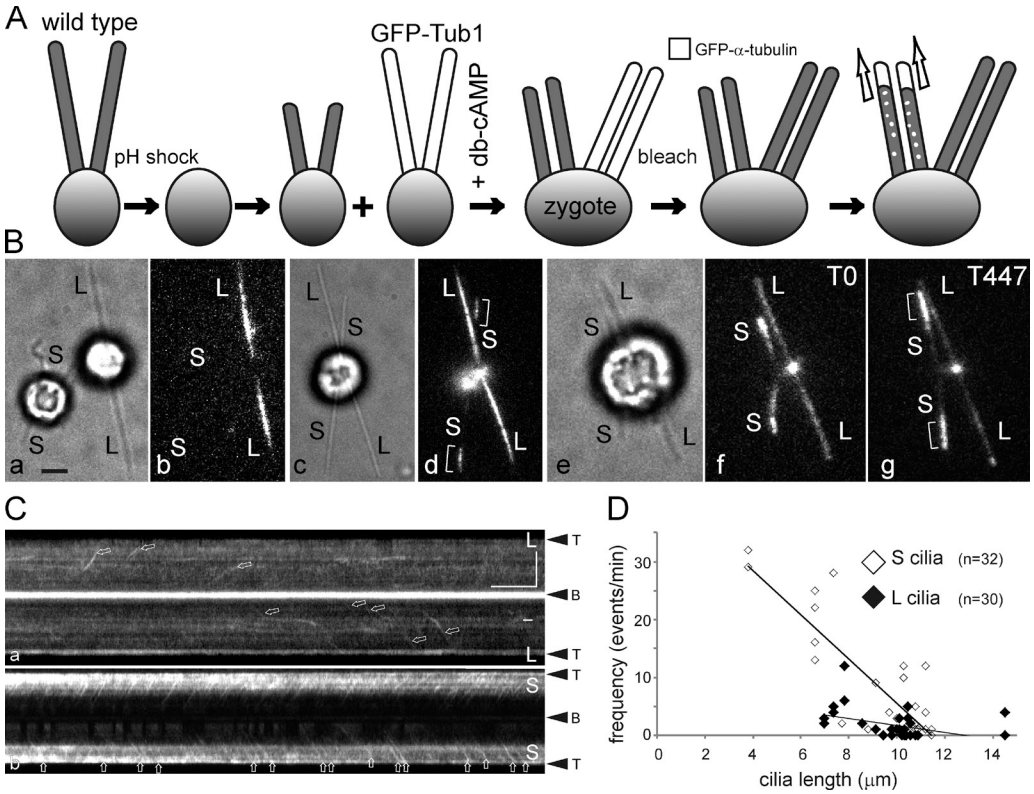

Figure 5. **Cells direct tubulin flux specifically into growing cilia.** (A) Schematic presentation of the experimental design. Wild-type gametes were deciliated by a pH shock, allowed to initiate cilia regeneration, and fused to GFP–α-tubulin expressing gametes with full-length cilia. Cell fusion was promoted by adding 15 mM dibutyryl cAMP (Pasquale and Goodenough, 1987). The resulting long-short zygotes will initially possess two short, regenerating cilia and two steady-state, GFP-positive cilia. To analyzed GFP-tubulin transport, all four cilia were photobleached. (B) Bright-field (a, c, and e) and TIRF images (b, d, f, and g) of gametes (a and b) and zygotes (c–g). S, regenerating cilia. L, long flagella derived from the GFP–α-tubulin donor strain. Brackets indicate ciliary segments assembled after cell fusion. Note elongation of short cilia depicted in e–g; the time points (in seconds) are indicated. Bar, 2 µm. (C) Kymograms of the long (L) and short (S) cilia of the zygote shown in B (e–g). Arrows: GFP-tubulin trajectories. Bars, 5 µm and 5 s. (D) Scatter plot showing the frequency of anterograde GFP-tubulin trajectories in wild-type–derived regenerating cilia (S cilia, open diamonds) and GFP-Tub1–derived cilia (L cilia, closed diamonds) of eight long-short zygotes. Mean values were 7.8 ± 10 versus 1.8 ± 2.6 events/min, respectively; P = 0.0016. Some data points with zero transport events and similar ciliary length overlap. See Fig. S4 for a histogram of the data.

As an alternative approach that does not require mechanical shearing, we generated long-short cells by mating GFP–α-tubulin–expressing gametes with full-length cilia to wild-type gametes that were deciliated by a pH shock and regenerating cilia (Fig. 5, A and B, a and b). The resulting zygotes, initially possessing two long GFP-positive and two short GFP-negative cilia, will equalize the length of all four cilia by partially resorbing the long ones and adding new tubulin to the short ones (Fig. 5 B, c–g; Ludington et al., 2012). Tubulin transport in all four cilia of such zygotes was analyzed after photobleaching (Fig. 5 C; Video 7). The frequency of tubulin transport by anterograde IFT in the short growing cilia surpassed that of the nongrowing long cilia (Fig. 5 D). As the four cilia approached equal length, the transport frequency in the initially long cilia increased, whereas that in the initially short ones decreased (Fig. S4 D). Based on the study of long-short cells, we conclude that the frequency of IFT-based tubulin transport events is controlled cilium-autonomously.

The concentration of soluble tubulin is increased during ciliary growth

In steady-state cilia, ∼10% of the total tubulin was in the detergent-soluble MM fraction (Fig. 1 D). The elongation of microtubules depends, among other factors, on the availability of αβ-tubulin dimers (Desai and Mitchison, 1997; Howard, 2001). Western blotting and FRAP analysis were used to test whether steady-state and growing cilia differ in the concentration of soluble tubulin. Steady-state, growing, and fully regenerated cilia were separated into axonemal and MM fractions; loading was adjusted to represent equal volumes of MM (Fig. 6 A). Western blots revealed that the amount of soluble tubulin was doubled from ∼10 to 20% of the total ciliary tubulin in growing versus nongrowing flagella (Fig. 6 A; for quantification see Fig. S4, B and C).

For FRAP analysis, ciliary segments were spot bleached (Video 8). An exchange of axonemal tubulin with GFP–α-tubulin laterally along the ciliary shaft was not observed in this study. Thus, axonemal GFP–α-tubulin will remain bleached. Soluble, unbleached GFP–α-tubulin from other ciliary segments or de novo imported from the cell body will move into the bleached region, and fluorescence recovery reflects the concentration of mobile GFP-tubulin in the cilium (Fig. 6 B). FRAP analysis showed recovery rates of 2 ± 1% of the pre-bleach fluorescence for nongrowing cilia (n = 16), whereas ∼15.6 ± 10% of the signal intensity recovered in growing cilia (n = 18; Fig. 6, C and D). In growing cilia, GFP-tubulin moving on IFT trains through the

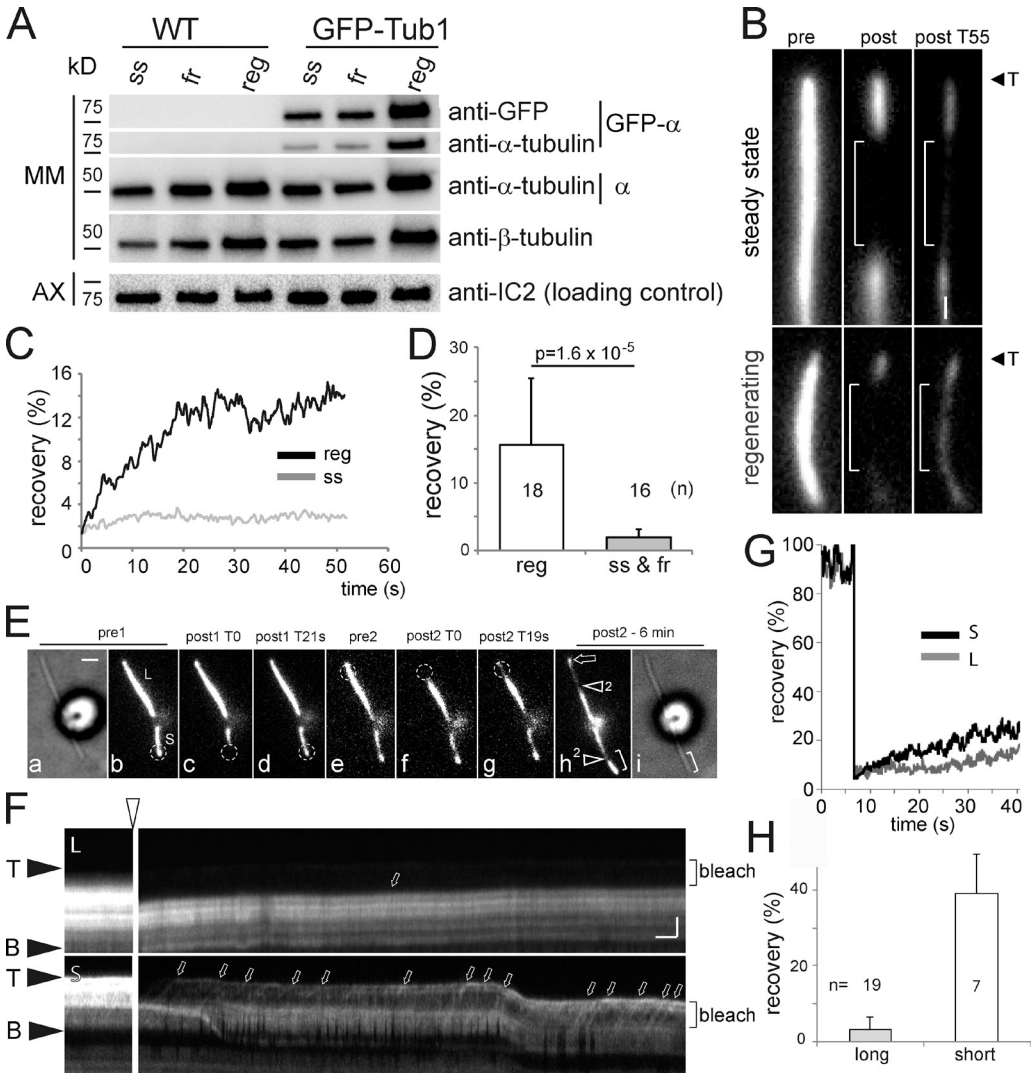

Figure 6. **The concentration of soluble tubulin is increased in growing cilia.** (A) Western blot comparing the amounts of tubulin in the MM fractions of steady-state (ss), fully regenerated (fr), and regenerating (reg) cilia. MM fractions were loaded to represent matching volumes of MM. Toward this end, loading was adjusted for equal amounts of axonemal proteins in the corresponding axonemal fractions based on anti-IC2 staining. See Fig. S4 D for quantification of band intensities. (B–D) FRAP analysis of steady-state and growing cilia. (B) After local bleaching of cilia using a focused laser beam (brackets), partial recovery of GFP–α-tubulin fluorescence was observed. Shown are images before (pre), and immediately (after T0) and 55 s (after T55) after photobleaching. Bar, 1 µm. (C) Single measurements of the fluorescence recovery (in % of the pre-bleaching intensity) in the bleached areas of a steady-state and a regenerating cilium. (D) Mean FRAP of regrowing (reg; $n = 18$) versus steady-state and fully regenerated (ss & fr; $n = 16$) cilia. Error bars indicate SEM. (E and F) FRAP analysis of a long-short cell. (E) Still images showing a long-short cell before (pre1) and immediately (post1 T0) and 21 s (post1 T21) after spot bleaching of the short cilium (S); pre2, post2 T0, and post2 T19 indicate similar steps for the long cilium. Dashed circle: position of the bleaching laser. Arrow in h: incorporation of GFP-tubulin into the long cilium. Arrowheads with 2 indicate additional areas bleached between post2 T19s and post2–6 min. Note considerable elongation of the initially short cilium (after 6 min; indicated by brackets). Bar, 2 µm. (F) Kymograms showing FRAP in the long (L) and the short (S) cilium of a given cell. Open arrowhead: bleaching steps. Small arrows: GFP–α-tubulin trajectories. Note recovery of a diffuse background of GFP–α-tubulin in the bottom panel. Bar, 2 µm and 2 s. (G) Single measurements of the fluorescence recovery (in percentage of the pre-bleaching intensity) in the bleached areas of the short and long cilia shown in F. (H) Mean FRAP of short and long cilia of long-short cells. Newly assembled axonemal segments (see brackets in E, h) were excluded from FRAP analysis. Error bars indicate SEM.

bleached region contributes to the recovery, but over time the diffused background staining significantly increased, indicating an increase in the concentration of GFP-tubulin diffusing inside cilia (Figs. 3 F, 6 F, and S5 B). Repeated bleaching of the same ciliary segment was followed by a recovery of similar strength (~5% for steady-state and ~15% for growing cilia; Fig. S5), indicative of an ongoing de novo import of GFP–α-tubulin into cilia.

An increase in the concentration of soluble tubulin in cilia could result from an increase in soluble tubulin in the cell body of regenerating cells. FRAP of long-short cells, however, showed that recovery was significantly stronger in the short cilium than in the long one (39 ± 10% vs. 4.3 ± 3%; Fig. 6, E–H; Fig. S5, C and D; Video 9). Thus, distinct concentrations of soluble tubulin can be established in the two cilia of the same cell. We conclude that the concentration of soluble tubulin is elevated in growing cilia. A high concentration of tubulin in the ciliary matrix is likely to promote elongation of the axonemal microtubules.

Defective regulation of tubulin transport in ciliary length mutants

Because microtubules are the major structural elements of cilia, defective regulation of tubulin transport could affect ciliary length. We expressed GFP–α-tubulin in *lf2-1* (*long flagella2*) and *shf2* (*short flagella2*) mutants and selected transformants expressing similar amounts of GFP-tubulin as the control strain GFP-Tub1 (Fig. S3 C). *lf2-1* has cilia of variable length with some 2–3× longer than wild type, whereas cilia reach only 6–8 µm in *shf2*. *LF2* encodes a CDK-like kinase, whereas the molecular defect in *shf2* is unknown (Kuchka and Jarvik, 1987; Tam et al., 2007). In steady-state *lf2-1* cilia, the mean frequency of GFP–α-tubulin transport was higher than in steady-state wild-type cilia; a length-dependent decrease in frequency was not observed (Fig. 7 A). Cilia regeneration in *lf2-1* was slow and irregular in onset with many cells failing to reassemble cilia (Barsel et al., 1988). In the *lf2-1* cells that regenerated cilia, the frequency of tubulin transport was somewhat higher but showed a similar lack of length dependency. The frequency of IFT was slightly reduced in *lf2-1* (unpublished data). *lf2-1* cells apparently fail to properly regulate the IFT-based transport of tubulin in response to changes in ciliary length.

In steady-state cilia of *shf2*, the frequency of tubulin transport decreased with increasing ciliary length and tubulin transport was rarely observed in *shf2* cilia longer than ∼6 µm, a length at which wild-type cilia showed robust trafficking of tubulin (Figs. 7 A and 3 D). IFT (based on DIC microscopy) appeared normal in the longer *shf2* cilia (unpublished data). Many *shf2* cells failed to regenerate cilia but the regrowth kinetics was largely normal in those that did (Kuchka and Jarvik, 1987). Regenerating *shf2* cilia showed a similar steep down-regulation of tubulin transport frequency with increasing ciliary length as described for *shf2* in steady-state. The data suggest that *shf2*, although able to increase tubulin transport frequency in short regenerating cilia, prematurely down-regulates tubulin transport by IFT. The data show that an abnormal regulation of tubulin transport occurs in mutants with defects in ciliary length regulation.

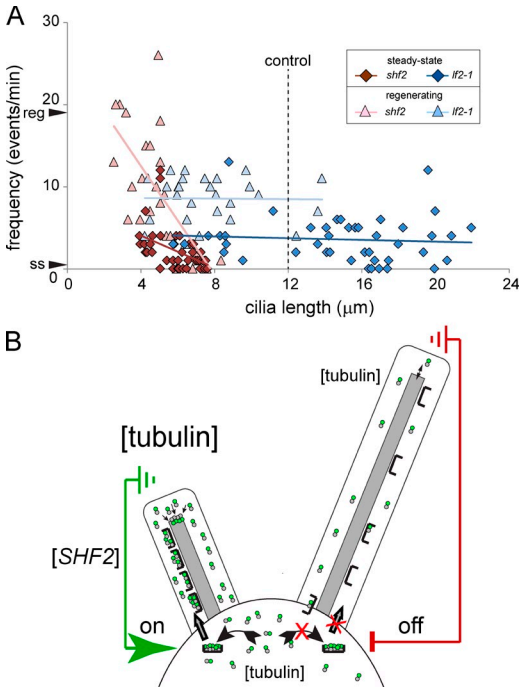

Figure 7. **Regulation of tubulin transport in cilia.** (A) Scatter plot of the frequencies of tubulin transport by anterograde IFT in *shf2* (red symbols) and *lf2-1* mutant cilia (blue symbols). Diamonds: steady-state cilia; triangles: regenerating cilia. Trend lines are given for each dataset. *n* = 27, 43, 29, and 44 for *lf2-1* regenerating and steady-state and *shf2* regenerating and steady-state, respectively, from a single experiment. The mean ciliary length of control cilia, and the frequencies of tubulin transport in steady-state and regenerating control cilia (arrowheads) are indicated. (B) Model of the regulation of tubulin transport. Incompletely assembled cilia (left) induce a signal resulting in increased loading of IFT particles with tubulin (curved arrow) or facilitated access of highly loaded IFT particles into cilia. Augmented tubulin transport will increase the concentration of soluble tubulin in the cilia matrix and promote the polymerization of axonemal microtubules. Mutants in *SHF2* prematurely down-regulate tubulin transport (A), suggesting that SHF2 functions in maintaining a high tubulin flux into cilia until steady-state length is reached. Full-length cilia (right) inhibit tubulin loading onto IFT or admission of highly loaded IFT trains into cilia.

Discussion

IFT functions as a tubulin transporter

Ciliary assembly requires a massive translocation of tubulin from the cell body into the growing organelle. In *C. reinhardtii*, almost 800,000 tubulin dimers, corresponding to ∼20% of the cell's total tubulin, are required to assemble its two 12-µm-long 9+2 cilia (Bhogaraju et al., 2014b; see Materials and methods). IFT is essential for the assembly of cilia and flagella in most eukaryotes and thought to be the major pathway of protein transport in cilia (Rosenbaum and Witman, 2002). Recent data, however, have shown that numerous proteins move into cilia in an IFT-independent manner. Ectopic cytosolic proteins up to a size of ∼50 kD enter cilia by passive diffusion; even proteins up to ∼650 kD appear to diffuse slowly into cilia (Kee et al., 2012; Breslow et al., 2013; Lin et al., 2013). In *C. reinhardtii*, the transmembrane protein SAG1 and the membrane-associated phospholipase D will enter cilia in the absence of IFT (Belzile et al., 2013; Lechtreck et al., 2013). Furthermore, certain transmembrane proteins (SSTR3, Smo) diffuse inside the ciliary membrane while associating only transiently—if ever—with IFT (Ye et al., 2013). These findings raised the question which proteins are the actual cargoes of IFT. Several TRP channels were reported to move by IFT and the BBSome cycles through cilia by associating to IFT trains (Blacque et al., 2004; Qin et al., 2004; Huang et al., 2007; Lechtreck et al., 2009). Also, IFT powers gliding and ciliary surface motility in *C. reinhardtii* presumably due to its interaction with the ciliary transmembrane protein FMG-1B (Collingridge et al., 2013; Shih et al., 2013). We recently showed that the axonemal proteins PF16, DRC2, and DRC4 are cargoes of IFT and that entry of DRC4-GFP into cilia is largely diminished in the absence of IFT (Wren et al., 2013). Defects in the IFT complex B protein IFT46 and or its interacting partner ODA16p largely prevent the transport of outer arm dynein to its ciliary docking sites (Hou et al., 2007; Ahmed et al., 2008). Thus, IFT plays a role in the transport of axonemal proteins, several of which are transported in large complexes feasibly rendering transport by diffusion inefficient. Several studies provided evidence that tubulin is a cargo of IFT but direct imaging of tubulin transport by

IFT and the quantification of such events has been challenging (Marshall and Rosenbaum, 2001; Hao et al., 2011; Bhogaraju et al., 2013; Brust-Mascher et al., 2013). Here, we show that GFP-tagged tubulin moves in association with IFT particles inside cilia indicating that IFT functions as tubulin transporter.

Cilium-autonomous regulation of tubulin transport by IFT

In growing cilia, the frequency of GFP-tubulin transport by IFT was greatly elevated. Taking into account that only a fraction of the total tubulin in cilia was tagged, extrapolation of the data indicates that IFT trains in growing cilia carry a larger tubulin load than those in steady-state cilia. Previously, we showed that the IFT-based transport of the axonemal protein DRC4 is strongly increased during ciliary growth (Wren et al., 2013). It is likely that the transport of many other ciliary proteins is also enhanced when cilia elongate. Although some differences in the velocity, size, and frequency of IFT in growing vs. steady-state cilia of *C. reinhardtii* have been reported, the number of IFT particles inside cilia is largely length-independent (Dentler, 2005; Marshall et al., 2005; Engel et al., 2009). In conclusion, IFT trains are highly loaded with cargo during ciliary growth; then, the number and velocity of IFT trains might limit the rate of ciliary elongation. Indeed, the 60% reduction in IFT frequency observed in the IFT kinesin mutant *fla3-1* results in sluggish regrowth of nearly full-length cilia (Mueller et al., 2005). In steady-state cilia, IFT particles carry less cargo probably running well below capacity. This would allow the cells to quickly adjust ciliary protein content and length in response to developmental or environmental cues by altering cargo loading of IFT (Wren et al., 2013).

Currently, it is unknown how the amount of cargo transported by IFT into cilia is regulated. In a simple model, an increase in the concentration of soluble tubulin in the cell body would make more tubulin available as cargo for IFT and promote tubulin transport into cilia (Chan and Marshall, 2012; Goehring and Hyman, 2012). Indeed, primary cilia elongate when the level of soluble cytoplasmic tubulin is increased by drug-induced microtubule depolymerization (Sharma et al., 2011). During ciliary growth, kinesin-13 may depolymerize cell body microtubules in *C. reinhardtii* to provide tubulin for axonemal assembly (Wang et al., 2013). Remarkably, in cells possessing growing and nongrowing cilia, the frequency of IFT-based GFP-tubulin transport was strongly elevated in the growing over the nongrowing cilia. We conclude that a general increase in tubulin supply in the cell body is insufficient to explain the increase in IFT-based tubulin transport just into growing cilia of long-short cells. Our data suggest that tubulin import into cilia is regulated locally within the basal body–cilium entity. An increase in admission of tubulin to the cilium could involve a change in the transition zone (TZ), located between the basal body and the cilium proper. TZ proteins are hotspots for ciliopathy-related mutations which alter the protein composition of cilia, and the TZ is thought to function as a ciliary gate regulating protein entry into the organelle (Craige et al., 2010; Omran, 2010; Williams et al., 2011; Kee and Verhey, 2013). The TZ could respond to changes in the ciliary length by permitting IFT particles carrying a large load into growing cilia while preventing such particles from entering steady-state cilia. Such a model of size-based exclusion of IFT trains at the TZ would require the constant presence of both loaded and unloaded IFT particles. The share of IFT trains occupied with GFP-tubulin in nongrowing and growing cilia ranges from <10 to ∼80%, rendering this model unlikely.

Alternatively, cargo loading onto IFT particles could be regulated. Dikaryon experiments showed that IFT proteins from distinct basal body–cilia units mix rapidly (Wren et al., 2013). Therefore, an increase in cargo loading onto IFT must happen locally at the base of a growing cilium, for example, by increasing the affinity of IFT carriers for cargo proteins. In C. *reinhardtii*, IFT particle and motor proteins are concentrated at the transitional fibers, which are located proximal to the TZ (Deane et al., 2001). The transitional fibers could increase the local concentration of IFT and cargoes and thereby promote the formation of IFT–cargo complexes. The anterograde IFT motor subunit KAP is more abundant at the base of growing cilia (Ludington et al., 2013), which might suggest that transitional fibers at the base of growing cilia have a higher capacity to bind IFT material. We propose a model in which cells measure the length of their cilia; cilia of insufficient length generate a signal that alters the property of the ciliary base, resulting in an increased loading of IFT particles and/or facilitated admission of highly loaded IFT trains into the cilium, which will augment the amount of tubulin transported into the cilium in need (Fig. 7 B).

Ciliary length defects are associated with dysregulation of tubulin transport

Sensing of ciliary length is likely to involve various protein kinases whose mutations lead to length defects (Berman et al., 2003; Tam et al., 2007; Lefebvre, 2009; Cao et al., 2013; Tam et al., 2013). LF2p, for example, is a CDK kinase which, together with LF1p and LF3p, forms the length regulating complex (LRC; Tam et al., 2007). LF2p homologues are also involved in ciliary length control in mammals and *C. elegans* (Ko et al., 2010; Phirke et al., 2011). In *lf2-1*, the frequency of tubulin transport was largely independent of ciliary length and remained elevated in *lf2-1* cilia that were longer than wild-type cilia. A failure to adjust tubulin transport with respect to ciliary length could explain the phenotype of *lf2-1* characterized by slow regeneration kinetics, and variable ciliary length with some abnormally long cilia (Barsel et al., 1988). The LRC is located in the cell body of *C. reinhardtii*, but its molecular role is unknown (Tam et al., 2007). Based on its localization, the LRC could function in adjusting IFT-based tubulin transport in response to signals from the ciliary length sensor.

Shorter-than-normal cilia could result from a failure to incorporate precursors into the cilium, an increased disassembly rate, or an insufficient delivery of precursors. The latter was observed in the short flagella mutant *shf2*. Tubulin transport was down-regulated well before cilia reached wild-type length. The phosphorylation pattern of the aurora-like kinase CALK can be used as an indicator of the assembly state of cilia. At the onset of ciliary growth, phosphorylation and dephosphorylation occur at distinct sites, followed by a gradual return to a pattern characteristic for full-length steady-state cilia (Luo et al., 2011; Cao

et al., 2013). *shf2* displays a CALK phosphorylation state typical for short, growing cilia (Luo et al., 2011; Cao et al., 2013). This suggests that *shf2* cells still sense the insufficient length of their cilia but fail to respond appropriately by maintaining a high tubulin influx via IFT.

In our study, we did not address the question of why the longer cilia of long-short cells retract. In those long cilia, tubulin transport via IFT—although well below that of short cilia—was actually somewhat above the steady-state levels (Fig. 4 C). Also, the breakdown of the axoneme is likely to increase the levels of soluble tubulin inside the shortening long cilia. Thus, ciliary shortening appears not to be driven by a shortage of tubulin, suggesting that the intraciliary tubulin concentration is not the sole factor regulating ciliary growth. We posit that the resorption involves an up-regulation of the cilia disassembly pathway in the long cilia. Putative players in the disassembly pathway are microtubule-destabilizing proteins such as kinesin-13 and CNK2. Mutants in the latter assemble the missing cilium of long-zero cells at normal rates but fail to resorb the remaining long cilium, supporting the notion that ciliary assembly and disassembly in long-short cells are distinctly regulated (Hilton et al., 2013).

IFT promotes ciliary growth by concentrating tubulin

GFP-tubulin enters cilia by both diffusion and IFT, raising the question of the respective roles in supplying tubulin for ciliary assembly. Tubulin dimers (110 kD) are above the predicted size exclusion limit of ∼50 kD for free diffusion of soluble protein into the cilium (Kee et al., 2012; Breslow et al., 2013). Distinct concentrations of soluble tubulin were observed in cilia of a given cell, indicating the absence of diffusive equilibration. We estimate (see Materials and methods) that the concentration of soluble tubulin in the ciliary matrix of growing cilia is higher than that in the cytoplasm; the absence of a cell body–to–cilia gradient in tubulin concentration rules out a net influx of tubulin into cilia by diffusion. In *fla10-1*, GFP-tubulin continued to enter cilia by diffusion in the absence of IFT but the cilia do not elongate. Similarly, ciliary elongation ceased in *shf2* after IFT of GFP-tubulin was down-regulated despite the continued entry of GFP-tubulin by diffusion. We conclude that the entry of tubulin into cilia by diffusion is insufficient to provide enough tubulin to promote ciliary growth.

Tubulin concentration has a strong impact on microtubule growth in vitro and in vivo, with high concentrations of tubulin suppressing catastrophe frequency and increasing the polymerization rate (Pedigo and Williams, 2002). In the cytoplasm, proteins such as XMAP215 act as microtubule polymerases at MT plus ends putatively by increasing the local tubulin dimer concentration (Al-Bassam and Chang, 2011). Messages of specific tubulin isoforms are recruited to microtubule plus-ends in the axonal growth cone to locally increase tubulin expression (Preitner et al., 2014). In growing cilia, large amounts of tubulin released from IFT into the cilium will increase the concentration of soluble tubulin in the matrix. We noticed a reduced mobility of tubulin in the vicinity of the ciliary tip, which could result from tubulin interactions with other proteins; IFT proteins, for example, are typically accumulated at the ciliary tip and possess tubulin binding motifs (Bhogaraju et al., 2014b). Further, GFP-tubulin was predominately released from IFT near the ciliary tip; reduced mobility and preferred unloading could further increase the tubulin concentration locally at the tip.

We predict that the concentration of soluble tubulin in the matrix of growing cilia is in the range of 300 µM (see Materials and methods). Although some of the tubulin is sequestered onto IFT, the concentration is well above the concentrations (∼20 µM) required for microtubule assembly in vitro or in the cytoplasm. *C. reinhardtii* cilia elongate at ∼350 nm/min compared with 20–60 µm/min observed for microtubules in the cytoplasm (Srayko et al., 2005). However, during axonemal assembly, nine doublet microtubules and two singlet microtubules are assembled simultaneously within the comparably small volume of the cilium. About 2,500 dimers are required to elongate a singlet microtubule by 20 µm, whereas the assembly of 350 nm of 9+2 microtubules consumes ∼10,000 dimers. We estimate ∼18,000 dimers to be present in the matrix of a 4-µm-long cilium (see Materials and methods). Thus, soluble tubulin in the ciliary matrix will be rapidly consumed during ciliary growth and the matrix pool must be equally rapidly replenished to ensure continued elongation of the axoneme. A unifying feature of most cilia is doublet microtubules, the assembly of which has not yet been reconstituted in vitro and could require very high concentrations of tubulin dimers. In summary, due to its architecture and its position within the small volume of the cilium, axonemal assembly could require exceptionally high concentrations of soluble tubulin. Several IFT complex B proteins contain tubulin-binding motifs—confirmed and predicted—and estimates suggest that IFT has the capacity to transport tubulin in amounts required during ciliary assembly (Bhogaraju et al., 2014). Although additional factors are likely involved in determining the rate of ciliary elongation (most notably the rate of axoneme depolymerization), tubulin transport by IFT and the resulting high concentration of tubulin in the ciliary matrix are likely prerequisites for the rapid elongation of axonemal microtubules. We propose that IFT functions as a tubulin pump to increase the concentration of tubulin inside growing cilia. Higher tubulin concentrations will promote the growth of the axonemal microtubules and thereby elongation of the cilium.

Materials and methods

Strains and culture conditions

C. reinhardtii cultures were maintained in modified M medium and aerated with 0.5% CO_2 at ∼21°C with a light/dark cycle of 14:10 h. To generate gametes, cells were grown on M plates for ∼7–10 d, placed into dim light for 2 d, and then incubated overnight in constant light in liquid M-N medium to induce gametogenesis. In mating reactions involving gametes with regenerating cilia, cell fusing was facilitated by addition of 15 mM dibutyryl-cAMP (Sigma-Aldrich; Pasquale and Goodenough, 1987).

Generation of transgenic strains

The vector pBR25 encoding mCerulean–α-tubulin downstream of the viral 2A sequence and the *BLE* selectable marker gene was provided by B. Rasala and S. Mayfield (University of California, San Diego, San Diego, CA). The humanized sfGFP gene was amplified by PCR using the primers 5′-CGCGGATCCATGGTGAGCAAGGGC-3′ and 5′-GCGGAATTCTTACTTGTACAGCTCGTCC-3′, digested with XhoI and BamH1 and ligated into pBR25 digested with the same enzymes; the mCerulean will be replaced with the sfGFP in the product. To generate mNeon-Green–tagged α-tubulin, the gene

was synthesized (Genewiz) using the *C. reinhardtii* codon usage and inserted into pBR25 as described above. α-Tubulin derivates were prepared as follows: gene segments encoding the modified C termini of α-tubulin were synthesized by Genewiz, excised with EcoRI and BglII, and ligated into pBR25-sfGFP vector digested with the same enzymes. Plasmids were restricted with KpnI and XbaI, and the gel-purified fragment encompassing the *BLE* and *TUA2* genes was transformed into *C. reinhardtii* by electroporation. Transformants were selected on TAP plates containing 10 µg/ml zeocin in constant light, transferred to liquid medium and analyzed by TIRF microscopy and Western blotting. The *ift20-1* IFT20-mCherry strain was generated by expressing the coding region of *IFT20* fused to mCherry under the control of the *FLA14* promoter in the *ift20-1* deletion mutant (Lechtreck et al., 2009); for double imaging the rescued *ift20-1* IFT20-mCherry strain was transformed again with the pBR-GFP–α-tubulin expression plasmid. The *fla10-1 ift20-1* IFT20-mCherry strain was generated by mating *fla10-1* and *ift20-1* IFT20-mCherry strains, followed by phenotypical and microscopic selection.

Isolation and fractionation of cilia

To isolate cilia for biochemical analysis, a protocol described by Witman (1986) was used. In brief, cells were concentrated and washed with 10 mM Hepes, pH 7.4. Cells were resuspended in HMS (10 mM Hepes, 5 mM $MgSO_4$, and 4% sucrose) and deciliated by adding dibucaine to a final concentration of 4.17 mM (Sigma-Aldrich). Cilia and cell bodies were separated by differential centrifugations and cilia were collected by sedimentation (17,000 *g*, 4°C, 20 min). Isolated cilia were resuspended in HMEK (30 mM HEPES, 5 mM $MgSO_4$, 0.5 mM EGTA, and 25 mM KCl) plus protease inhibitor (P9599; 1:100; Sigma-Aldrich) and demembranated by addition of 1% NP-40 Alternative (final concentration; EMD Millipore) on ice for 20 min. Axonemes were pelleted by centrifugation (30,000 *g*, 4°C, 20 min) and fractions were analyzed by SDS-PAGE and Western blotting.

Flagellar regeneration and generation of long-short cells

Cells in M were deflagellated by pH shock, transferred to fresh M medium, and allowed to regrow cilia under constant light with agitation (Lefebvre, 1995). To delay the onset on regeneration, cells were kept on wet ice until needed. For long-short experiments, cells were passed 4–6× through a 26G × 1/2 needle using a 1-ml syringe, which resulted in a small percentage of long-zero cells. In experiments involving CHX, 10 µM CHX was added to the cells ∼30 min before pH shock and cells were resuspended in fresh M medium supplemented with 10 µM CHX after pH shock. Cells were allowed to regenerate for 20 min at RT or 16°C, and then aliquots were transferred to 32°C for >180 min to inactivate IFT in *fla10-1* strains.

TIRF microscopy

A microscope (Eclipse Ti-U; Nikon) equipped with 60× NA1.49 TIRF objective and through-the-objective TIRF illumination provided by a 40-mW 488-nm and a 75-mW 561-nm diode laser (Spectraphysics) was used for in vivo imaging (Lechtreck, 2013). The excitation lasers were cleaned up with a Nikon GFP/mCherry TIRF filter and the emission was separated using an Image Splitting Device (Photometrics DualView2 with filter cube 11-EM). Observation chambers were assembled by inverting a 22 × 22 mm no. 1.5 cover glass with ∼10 µl of 5 mM Hepes, pH 7.3, 6.25 mM EGTA onto an equal volume of cells in M medium on a 24 × 60 mm no. 1.5 cover glass. Cells were imaged through the large cover glass at room temperature or, for temperature-sensitive experiments, at 32°C using a Bioptechs objective heater. Images were recorded at 2–31 fps using an iXON3 (Andor) and the NIS-Elements Advanced Research software (Nikon). ImageJ (National Institutes of Health) with the LOCI plugin (University of Wisconsin, Madison WI) and multiple kymogram plugin (European Molecular Biology Laboratory) were used to generate kymograms as described in Lechtreck (2013). Videos were generated by adjusting image contrast in ImageJ. Images were then cropped, rotated, converted to 8-bit in ImageJ, and exported in AVI format; QuickTime was used for scene selection. Individual frames were copied into Photoshop (Adobe) and adjusted for contrast and brightness; figures were assembled in Illustrator (CS6 version 16.0.3; Adobe). For photobleaching of the entire cilia, the intensity of the 488-nm laser was increased to 10% or more for 4–12 s. Partial bleaching of the cilia was achieved by using a focused 488-nm laser beam in epifluorescence; near complete bleaching of a 3-µm diameter region was accomplished in 50–300 ms.

FRAP analysis

Videos were opened in ImageJ, a region of interest (ROI) encompassing the central part of the bleached region was selected using the *Rectangular* tool, fluorescence intensities in the ROIs were determined using the *Plot z-axis Profile* tool, and the values were exported into Excel. Data of each frame were corrected for background fluorescence. The pre-bleach signal within the bleached ROI was set to 100% and the recovery (in percentage of the pre-bleach signal) was calculated. The distal regions of growing cilia were excluded from the ROIs used for recovery analysis. GFP–α-tubulin incorporated into the axoneme cannot recover and will lose fluorescence intensity with time. In contrast, soluble tubulin in the matrix will perpetually reenter cilia and the bleached areas. This will lead to an apparent increase of signal intensity in the FRAP areas compared with the unbleached areas. Correction of FRAP data for loss of fluorescence in unbleached control regions was therefore omitted.

Calculation of the diffusion coefficient of GFP–α-tubulin

To determine the diffusion coefficient of GFP–α-tubulin, we followed the method described for DRC4-GFP (Wren et al., 2013). In brief, 10 videos were selected based on their kymograms which showed many trajectories of diffusing particles. Trajectories were then identified from each video using the ImageJ plug-in Mosaic Particle Tracker (Sbalzarini and Koumoutsakos, 2005). The coefficients used in the particle tracker were the following: kernel radius 2, cutoff radius 3.0, percentile 0.2, displacement 5.0, and link range 5.

We calculated the mean square displacement versus time for all trajectories longer than 3 s (30 time points) according to the method of Qian et al. (1991). For the time point n, corresponding to a time $t = n\Delta T$, the mean square displacements in the x and y dimensions are calculated for each trajectory, j, as

$$\rho_{x,j}(n) = \frac{1}{N_{j,n}+1}\sum_{i=0}^{N_{j,n}}\left(x_{i+n}-x_i\right)^2$$

and

$$\rho_{y,j}(n) = \frac{1}{N_{j,n}+1}\sum_{i=0}^{N_{j,n}}\left(y_{i+n}-y_i\right)^2,$$

where $N_{j,n}$ is the number of values calculated for the j[th] trajectory and n[th] time point; for shorter times, $N_{j,n}$ will be larger because there will be more pairs of points separated by n. The x and y dimensions are defined along the camera axes, not in relation to the cilia. The mean square displacement along the cilia is $\rho_j(n) = \rho_{x,j}(n) + \rho_{y,j}(n)$. The mean square displacements for all the trajectories are then combined:

$$\rho(n) = \frac{1}{1+\sum N_{j,n}}\sum_j\left(N_{j,n}+1\right)\rho_j(n).$$

Custom programs were written in Matlab to read the trajectories produced by the Mosaic Particle Tracker and perform the above analysis.

This resulted in 64 trajectories being analyzed. A linear fit to the first six data points (the first 0.5 s) yields a slope of 3.13 ± 0.20 µm^2/s, corresponding to a 1D diffusion coefficient of 1.76 ± 0.18 µm^2/s. The uncertainty of each data point is calculated as the standard error of the mean. Similarly, we analyzed GFP–α-tubulin particles diffusing with reduced mobility in the vicinity of the ciliary tip (1D diffusion coefficient 0.2 µm^2/s based on 58 trajectories from 12 videos). In detail, an area containing ∼1 µm at the tip of the cilia was cut out. Trajectories were then identified as described for diffusion along the cilia body. We calculated the mean square displacement versus time for all trajectories longer than 1s (corresponding to 10 time points at 10 fps). Trajectories in which the particle's mean movement was <0.1 µm in 100 ms were excluded from further analysis because these might present particles stably incorporated into the axoneme. This resulted in 58 trajectories being analyzed. A linear fit to the first six data points yields a slope of 0.3644 ± 0.044 µm^2/s, corresponding to a 1D diffusion coefficient of 0.18 ± 0.02 µm^2/s.

Immunoprecipitation of GFP–α-tubulin

Cilia were isolated from the GFP–α-tubulin–expressing strain GFP-Tub1 and a wild-type control strain, resuspended in HMEK (30 mM Hepes, 5 mM $MgSO_4$, 0.5 mM EGTA, and 25 mM KCl) plus protease inhibitor cocktail and lysed by adding an equal volume of HMEK supplemented with 250 mM NaCl and 0.5% NP-40; axonemes were removed by centrifugation (20,000 *g*, 4°C, 10 min). The MM fractions were incubated for 1 h at 5°C with agitation with anti-GFP agarose beads (GFP-nAb; Allele Biotechnology) pretreated with 5% BSA. After several washes with HMEK supplemented with

250 mM NaCl, the beads were eluted using 1 M glycine, pH 2.5. The eluted proteins were then analyzed by SDS-PAGE followed by silver staining (Bio-Rad Laboratories) and Western blotting.

Western blotting

Flagellar proteins were separated by SDS-PAGE and transferred to PVDF membrane (Immobilon; Millipore) using standard protocols. The following primary antibodies were used: mouse anti-acetylated tubulin (clone 6-11B-1; 1:10,000; Sigma-Aldrich), mouse anti–α-tubulin (clone B-5-1-2; 1:10,000; Sigma-Aldrich), mouse anti-IC2 (1:50; King and Witman, 1990), mouse anti-IFT81 (1:200; Cole et al., 1998), mouse anti-IFT139 (1:50; Cole et al., 1998), and mouse anti-IFT172 (1:50; Cole et al., 1998), mouse GT335 (anti-glutamylated tubulin; 1:2,000; AdipoGen), rabbit anti–β-tubulin (1:2,000; Silflow and Rosenbaum, 1981), rabbit anti-FAP12 (1:1,000; provided by D. Cole, University of Idaho, Moscow, ID), rabbit anti-GFP (1:500; Invitrogen), and rabbit anti-NAB1 (1:5,000; Agrisera). Western blots were developed using anti–mouse or anti–rabbit secondary antibodies conjugated to horseradish peroxidase (Molecular Probes) and chemiluminescence substrate (SuperSignal West Dura; Thermo Fisher Scientific). A ChemiDoc MP imaging system was used for imaging and Image Lab (both Bio-Rad Laboratories) was used for signal quantification.

Calculation of the concentration of tubulin in the ciliary matrix

The axoneme contains 11 microtubules with 13 protofilaments and 9 B-tubules with 10 protofilaments. The length of an αβ-tubulin dimer is ∼8 nm and ∼350,000 dimers are required to assemble one axoneme of 12-µm length. Approximately 10% of the total ciliary tubulin is in the MM fraction suggesting a total of ∼380,000 tubulin dimers per cilium. Cilia have a diameter of 250 nm and the volume of a cilium of 12-µm length is 0.75 μm^3 or 0.75×10^{-15} liters. Thus, the total tubulin concentration in cilia is around 0.9 mM which is ∼40× higher than the 24 µM reported for *Xenopus* egg extracts (Gard and Kirschner, 1987). Based on unstained cross sections through cilia, we estimate that the ciliary axoneme occupies ∼50% of the ciliary volume; then, the tubulin concentration in the ciliary matrix is ∼160 µM during steady-state. FRAP analysis of GFP-tubulin revealed a significant increase of free tubulin in the matrix of growing cilia and Western blotting indicated that the concentration of soluble tubulin in growing cilia is about twice as high as that of steady-state cilia corresponding to ∼320 µM.

For the ovoid cell bodies of *C. reinhardtii*, we estimated a volume of 251 μm^3 or 2.5×10^{-13} liters, using a length of 10 µm, a height of 6 µm, and a width of 8 µm. Ciliary tubulin amounts to ∼20% of the total tubulin in whole cells ($\sim 4 \times 10^6$ tubulin dimers) indicating $\sim 3.2 \times 10^6$ dimers corresponding to a concentration of ∼20 µM to be present in the cell body. However, this value is misleading because cell bodies, in contrast to most cilia, contain membrane-enclosed spaces (plastids, mitochondria, vesicles etc.) which are not accessible to tubulin. Assuming that 20% of the cellular space in *C. reinhardtii* is accessible to tubulin, the tubulin concentration would increase to 120 µM. In mammalian cells, ∼30–50% of the tubulin in the cell body is soluble (Sharma et al., 2011). The microtubular cytoskeleton of *C. reinhardtii* cell bodies consists of the two flagellar-bearing basal bodies of 250-nm length with triplet microtubules, two short nascent basal bodies, 12 rootlet microtubules organized into four bundles, two consisting of 2 and two consisting of 4 microtubules, and an unknown number of so-called secondary cytoplasmic microtubules. Assuming that ∼40% of the tubulin in the cell body of *C. reinhardtii* is soluble, the concentration of soluble tubulin in the cell body cytoplasm would be ∼50 µM. Even taking into account that during ciliary generation some of the cytoplasmic microtubules are shortened and tubulin expression is up-regulated, we consider it unlikely that the concentration of soluble tubulin in the cell body will exceed a concentration of 320 µM calculated for the matrix of growing cilia. Although there are numerous uncertainties in this estimate, we consider the presence of a gradient in tubulin concentration from the cell body to cilium improbable. Such a gradient would be required for an efficient diffusion-driven net influx of tubulin into cilia. In conclusion, active transport in the form of IFT is required to concentrate tubulin in the ciliary matrix.

Online supplemental material

Fig. S1 shows the coimmunoprecipitation of GFP—α-tubulin with endogenous β-tubulin from the ciliary matrix. Fig. S2 is a gallery of kymograms of GFP-tubulin transport. Fig. S3 shows Western blot analyses of strains used in this study. Fig. S4 provides supplementary data on the IFT occupancy, the amount of soluble tubulin in cilia, and tubulin transport in long-short zygotes. Fig. S5 shows FRAP analyses of steady-state, growing, and long-short cilia. The supplemental videos show TIRF recordings of fluorescent protein-tagged α-tubulin in *C. reinhardtii* cilia during anterograde transport (Video 1), while diffusing along the ciliary shaft (Video 2), during active transport together with IFT20-mCherry as a marker for IFT (Video 3), while diffusing near the ciliary tip with reduced mobility (Video 4), during ciliary assembly (Video 5), during assembly of just one cilium of a long-short cell (Video 6), during ciliary assembly in a zygote with two growing and two nongrowing cilia (Video 7), while reentering a bleached area of a steady-state cilium by diffusion (Video 8), and while reentering bleached areas in the long and in the short cilium of a long-short cell (Video 9). Table S1 shows that the E-hook of α-tubulin is not required for transport via IFT. The following Matlab source codes are available in the supplemental materials: tracksxml.m will read in data from an xml file generated by the Mosaic Particle Tracker; traj_anal.m to perform a quick analysis of particle track data, it will generate some values related to whether the particle is likely diffusing or moving at a constant velocity; traj_stats.m to perform diffusion analysis (mean square distance vs. time); and trajectories_folder.m to perform diffusion analysis of a list of xml files generated by the Mosaic Particle Tracker. Online supplemental material is available at http://www.jcb.org/cgi/content/full/jcb.201409036/DC1.

We are grateful to Dr. Jaçek Gaertig (University of Georgia) for helpful discussions and critical reading of the manuscript, Drs. Beth Rasala and Steve Mayfield (University of California, San Diego) for providing plasmids to express fluorescent tubulin, Dr. Ahmet Yildiz (University of California, Berkeley) for advice on the installation the spot bleaching laser, and Dr. Doug Cole (University of Idaho) for the gift of anti-FAP12 antibody.

This work was support by a grant from the National Institutes of Health (GM110413), a pilot grant from the University of Alabama Hepato-Renal Fibrocystic Disease Core Center (National Institutes of Health 5P30DK074038-09, subaward number: 0004392208-003), and by start-up funding from the University of Georgia to K. Lechtreck.

The authors declare no competing financial interests.

Submitted: 8 September 2014
Accepted: 15 December 2014

References

Ahmed, N.T., C. Gao, B.F. Lucker, D.G. Cole, and D.R. Mitchell. 2008. ODA16 aids axonemal outer row dynein assembly through an interaction with the intraflagellar transport machinery. *J. Cell Biol.* 183:313–322. http://dx.doi.org/10.1083/jcb.200802025

Al-Bassam, J., and F. Chang. 2011. Regulation of microtubule dynamics by TOG-domain proteins XMAP215/Dis1 and CLASP. *Trends Cell Biol.* 21:604–614. http://dx.doi.org/10.1016/j.tcb.2011.06.007

Barsel, S.E., D.E. Wexler, and P.A. Lefebvre. 1988. Genetic analysis of long-flagella mutants of *Chlamydomonas reinhardtii*. *Genetics*. 118:637–648.

Belzile, O., C.I. Hernandez-Lara, Q. Wang, and W.J. Snell. 2013. Regulated membrane protein entry into flagella is facilitated by cytoplasmic microtubules and does not require IFT. *Curr. Biol.* 23:1460–1465. http://dx.doi.org/10.1016/j.cub.2013.06.025

Berman, S.A., N.F. Wilson, N.A. Haas, and P.A. Lefebvre. 2003. A novel MAP kinase regulates flagellar length in *Chlamydomonas*. *Curr. Biol.* 13:1145–1149. http://dx.doi.org/10.1016/S0960-9822(03)00415-9

Bhogaraju, S., L. Cajanek, C. Fort, T. Blisnick, K. Weber, M. Taschner, N. Mizuno, S. Lamla, P. Bastin, E.A. Nigg, and E. Lorentzen. 2013. Molecular basis of tubulin transport within the cilium by IFT74 and IFT81. *Science*. 341:1009–1012. http://dx.doi.org/10.1126/science.1240985

Bhogaraju, S., K. Weber, B.D. Engel, K.F. Lechtreck, and E. Lorentzen. 2014. Getting tubulin to the tip of the cilium: one IFT train, many different tubulin cargo-binding sites? *BioEssays*. 36:463–467. http://dx.doi.org/10.1002/bies.201400007

Blacque, O.E., M.J. Reardon, C. Li, J. McCarthy, M.R. Mahjoub, S.J. Ansley, J.L. Badano, A.K. Mah, P.L. Beales, W.S. Davidson, et al. 2004. Loss of *C. elegans* BBS-7 and BBS-8 protein function results in cilia defects and compromised intraflagellar transport. *Genes Dev.* 18:1630–1642. http://dx.doi.org/10.1101/gad.1194004

Borisy, G.G., and E.W. Taylor. 1967. The mechanism of action of colchicine. Binding of colchicine-3H to cellular protein. *J. Cell Biol.* 34:525–533. http://dx.doi.org/10.1083/jcb.34.2.525

Breslow, D.K., E.F. Koslover, F. Seydel, A.J. Spakowitz, and M.V. Nachury. 2013. An in vitro assay for entry into cilia reveals unique properties of the soluble diffusion barrier. *J. Cell Biol.* 203:129–147. http://dx.doi.org/10.1083/jcb.201212024

Brust-Mascher, I., G. Ou, and J.M. Scholey. 2013. Measuring rates of intraflagellar transport along *Caenorhabditis elegans* sensory cilia using fluorescence

microscopy. *Methods Enzymol.* 524:285–304. http://dx.doi.org/10.1016/B978-0-12-397945-2.00016-0

Cao, M., D. Meng, L. Wang, S. Bei, W.J. Snell, and J. Pan. 2013. Activation loop phosphorylation of a protein kinase is a molecular marker of organelle size that dynamically reports flagellar length. *Proc. Natl. Acad. Sci. USA*. 110:12337–12342. http://dx.doi.org/10.1073/pnas.1302364110

Chan, Y.H., and W.F. Marshall. 2012. How cells know the size of their organelles. *Science*. 337:1186–1189. http://dx.doi.org/10.1126/science.1223539

Cole, D.G., D.R. Diener, A.L. Himelblau, P.L. Beech, J.C. Fuster, and J.L. Rosenbaum. 1998. *Chlamydomonas* kinesin-II-dependent intraflagellar transport (IFT): IFT particles contain proteins required for ciliary assembly in *Caenorhabditis elegans* sensory neurons. *J. Cell Biol.* 141:993–1008. http://dx.doi.org/10.1083/jcb.141.4.993

Collingridge, P., C. Brownlee, and G.L. Wheeler. 2013. Compartmentalized calcium signaling in cilia regulates intraflagellar transport. *Curr. Biol.* 23:2311–2318. http://dx.doi.org/10.1016/j.cub.2013.09.059

Craige, B., C.C. Tsao, D.R. Diener, Y. Hou, K.F. Lechtreck, J.L. Rosenbaum, and G.B. Witman. 2010. CEP290 tethers flagellar transition zone microtubules to the membrane and regulates flagellar protein content. *J. Cell Biol.* 190:927–940. http://dx.doi.org/10.1083/jcb.201006105

Deane, J.A., D.G. Cole, E.S. Seeley, D.R. Diener, and J.L. Rosenbaum. 2001. Localization of intraflagellar transport protein IFT52 identifies basal body transitional fibers as the docking site for IFT particles. *Curr. Biol.* 11:1586–1590. http://dx.doi.org/10.1016/S0960-9822(01)00484-5

Dentler, W. 2005. Intraflagellar transport (IFT) during assembly and disassembly of *Chlamydomonas flagella*. *J. Cell Biol.* 170:649–659. http://dx.doi.org/10.1083/jcb.200412021

Desai, A., and T.J. Mitchison. 1997. Microtubule polymerization dynamics. *Annu. Rev. Cell Dev. Biol.* 13:83–117. http://dx.doi.org/10.1146/annurev.cellbio.13.1.83

Duan, J., and M.A. Gorovsky. 2002. Both carboxy-terminal tails of alpha- and beta-tubulin are essential, but either one will suffice. *Curr. Biol.* 12:313–316. http://dx.doi.org/10.1016/S0960-9822(02)00651-6

Engel, B.D., W.B. Ludington, and W.F. Marshall. 2009. Intraflagellar transport particle size scales inversely with flagellar length: revisiting the balance-point length control model. *J. Cell Biol.* 187:81–89. http://dx.doi.org/10.1083/jcb.200812084

Euteneuer, U., and J.R. McIntosh. 1981. Polarity of some motility-related microtubules. *Proc. Natl. Acad. Sci. USA*. 78:372–376. http://dx.doi.org/10.1073/pnas.78.1.372

Gaertig, J., and D. Wloga. 2008. Ciliary tubulin and its post-translational modifications. *Curr. Top. Dev. Biol.* 85:83–113. http://dx.doi.org/10.1016/S0070-2153(08)00804-1

Gard, D.L., and M.W. Kirschner. 1987. Microtubule assembly in cytoplasmic extracts of *Xenopus* oocytes and eggs. *J. Cell Biol.* 105:2191–2201. http://dx.doi.org/10.1083/jcb.105.5.2191

Goehring, N.W., and A.A. Hyman. 2012. Organelle growth control through limiting pools of cytoplasmic components. *Curr. Biol.* 22:R330–R339. http://dx.doi.org/10.1016/j.cub.2012.03.046

Hao, L., M. Thein, I. Brust-Mascher, G. Civelekoglu-Scholey, Y. Lu, S. Acar, B. Prevo, S. Shaham, and J.M. Scholey. 2011. Intraflagellar transport delivers tubulin isotypes to sensory cilium middle and distal segments. *Nat. Cell Biol.* 13:790–798. http://dx.doi.org/10.1038/ncb2268

Hilton, L.K., K. Gunawardane, J.W. Kim, M.C. Schwarz, and L.M. Quarmby. 2013. The kinases LF4 and CNK2 control ciliary length by feedback regulation of assembly and disassembly rates. *Curr. Biol.* 23:2208–2214. http://dx.doi.org/10.1016/j.cub.2013.09.038

Hou, Y., H. Qin, J.A. Follit, G.J. Pazour, J.L. Rosenbaum, and G.B. Witman. 2007. Functional analysis of an individual IFT protein: IFT46 is required for transport of outer dynein arms into flagella. *J. Cell Biol.* 176:653–665. http://dx.doi.org/10.1083/jcb.200608041

Howard, J. 2001. Mechanics of motor proteins and the cytoskeleton. Sinauer Associates, Publishers, Sunderland, Mass. 67 pp.

Huang, K., D.R. Diener, A. Mitchell, G.J. Pazour, G.B. Witman, and J.L. Rosenbaum. 2007. Function and dynamics of PKD2 in *Chlamydomonas reinhardtii* flagella. *J. Cell Biol.* 179:501–514. http://dx.doi.org/10.1083/jcb.200704069

Johnson, K.A., and J.L. Rosenbaum. 1992. Polarity of flagellar assembly in *Chlamydomonas*. *J. Cell Biol.* 119:1605–1611. http://dx.doi.org/10.1083/jcb.119.6.1605

Kee, H.L., and K.J. Verhey. 2013. Molecular connections between nuclear and ciliary import processes. *Cilia*. 2:11. http://dx.doi.org/10.1186/2046-2530-2-11

Kee, H.L., J.F. Dishinger, T.L. Blasius, C.J. Liu, B. Margolis, and K.J. Verhey. 2012. A size-exclusion permeability barrier and nucleoporins characterize a ciliary pore complex that regulates transport into cilia. *Nat. Cell Biol.* 14:431–437. http://dx.doi.org/10.1038/ncb2450

King, S.M., and G.B. Witman. 1990. Localization of an intermediate chain of outer arm dynein by immunoelectron microscopy. *J. Biol. Chem.* 265:19807–19811.

Ko, H.W., R.X. Norman, J. Tran, K.P. Fuller, M. Fukuda, and J.T. Eggenschwiler. 2010. Broad-minded links cell cycle-related kinase to cilia assembly and hedgehog signal transduction. *Dev. Cell*. 18:237–247. http://dx.doi.org/10.1016/j.devcel.2009.12.014

Kozminski, K.G., K.A. Johnson, P. Forscher, and J.L. Rosenbaum. 1993. A motility in the eukaryotic flagellum unrelated to flagellar beating. *Proc. Natl. Acad. Sci. USA*. 90:5519–5523. http://dx.doi.org/10.1073/pnas.90.12.5519

Kozminski, K.G., P.L. Beech, and J.L. Rosenbaum. 1995. The *Chlamydomonas* kinesin-like protein FLA10 is involved in motility associated with the flagellar membrane. *J. Cell Biol.* 131:1517–1527. http://dx.doi.org/10.1083/jcb.131.6.1517

Kuchka, M.R., and J.W. Jarvik. 1987. Short-Flagella Mutants of *Chlamydomonas reinhardtii*. *Genetics*. 115:685–691.

Lechtreck, K.F. 2013. In vivo imaging of IFT in *Chlamydomonas* flagella. *Methods Enzymol.* 524:265–284. http://dx.doi.org/10.1016/B978-0-12-397945-2.00015-9

Lechtreck, K.F., E.C. Johnson, T. Sakai, D. Cochran, B.A. Ballif, J. Rush, G.J. Pazour, M. Ikebe, and G.B. Witman. 2009. The *Chlamydomonas reinhardtii* BBSome is an IFT cargo required for export of specific signaling proteins from flagella. *J. Cell Biol.* 187:1117–1132. http://dx.doi.org/10.1083/jcb.200909183

Lechtreck, K.F., J.M. Brown, J.L. Sampaio, J.M. Craft, A. Shevchenko, J.E. Evans, and G.B. Witman. 2013. Cycling of the signaling protein phospholipase D through cilia requires the BBSome only for the export phase. *J. Cell Biol.* 201:249–261. http://dx.doi.org/10.1083/jcb.201207139

Lefebvre, P.A. 1995. Flagellar amputation and regeneration in *Chlamydomonas*. *Methods Cell Biol.* 47:3–7. http://dx.doi.org/10.1016/S0091-679X(08)60782-7

Lefebvre, P.A. 2009. Flagellar length control. *In* The *Chlamydomonas* sourcebook, Vol. 3: Cell motility and behavior. E.H. Harris and G.B. Witmann, editors. Elsevier, Amsterdam, 115–129.

Lin, Y.C., P. Niewiadomski, B. Lin, H. Nakamura, S.C. Phua, J. Jiao, A. Levchenko, T. Inoue, R. Rohatgi, and T. Inoue. 2013. Chemically inducible diffusion trap at cilia reveals molecular sieve-like barrier. *Nat. Chem. Biol.* 9:437–443. http://dx.doi.org/10.1038/nchembio.1252

Ludington, W.B., L.Z. Shi, Q. Zhu, M.W. Berns, and W.F. Marshall. 2012. Organelle size equalization by a constitutive process. *Curr. Biol.* 22:2173–2179. http://dx.doi.org/10.1016/j.cub.2012.09.040

Ludington, W.B., K.A. Wemmer, K.F. Lechtreck, G.B. Witman, and W.F. Marshall. 2013. Avalanche-like behavior in ciliary import. *Proc. Natl. Acad. Sci. USA*. 110:3925–3930. http://dx.doi.org/10.1073/pnas.1217354110

Luo, M., M. Cao, Y. Kan, G. Li, W. Snell, and J. Pan. 2011. The phosphorylation state of an aurora-like kinase marks the length of growing flagella in Chlamydomonas. *Curr. Biol.* 21:586–591. http://dx.doi.org/10.1016/j.cub.2011.02.046

Mahjoub, M.R., and T. Stearns. 2012. Supernumerary centrosomes nucleate extra cilia and compromise primary cilium signaling. *Curr. Biol.* 22:1628–1634. http://dx.doi.org/10.1016/j.cub.2012.06.057

Mahjoub, M.R., M.L. Trapp, and L.M. Quarmby. 2005. NIMA-related kinases defective in murine models of polycystic kidney diseases localize to primary cilia and centrosomes. *J. Am. Soc. Nephrol.* 16:3485–3489. http://dx.doi.org/10.1681/ASN.2005080824

Marshall, W.F., and J.L. Rosenbaum. 2001. Intraflagellar transport balances continuous turnover of outer doublet microtubules: implications for flagellar length control. *J. Cell Biol.* 155:405–414. http://dx.doi.org/10.1083/jcb.200106141

Marshall, W.F., H. Qin, M. Rodrigo Brenni, and J.L. Rosenbaum. 2005. Flagellar length control system: testing a simple model based on intraflagellar transport and turnover. *Mol. Biol. Cell*. 16:270–278. http://dx.doi.org/10.1091/mbc.E04-07-0586

Mueller, J., C.A. Perrone, R. Bower, D.G. Cole, and M.E. Porter. 2005. The FLA3 KAP subunit is required for localization of kinesin-2 to the site of flagellar assembly and processive anterograde intraflagellar transport. *Mol. Biol. Cell*. 16:1341–1354. http://dx.doi.org/10.1091/mbc.E04-10-0931

Omran, H. 2010. NPHP proteins: gatekeepers of the ciliary compartment. *J. Cell Biol.* 190:715–717. http://dx.doi.org/10.1083/jcb.201008080

Özgül, R.K., A.M. Siemiatkowska, D. Yücel, C.A. Myers, R.W. Collin, M.N. Zonneveld, A. Beryozkin, E. Banin, C.B. Hoyng, L.I. van den Born, et al. European Retinal Disease Consortium. 2011. Exome sequencing and cis-regulatory mapping identify mutations in MAK, a gene encoding a regulator of ciliary length, as a cause of retinitis pigmentosa. *Am. J. Hum. Genet.* 89:253–264. http://dx.doi.org/10.1016/j.ajhg.2011.07.005

Pasquale, S.M., and U.W. Goodenough. 1987. Cyclic AMP functions as a primary sexual signal in gametes of *Chlamydomonas reinhardtii*. *J. Cell Biol.* 105:2279–2292. http://dx.doi.org/10.1083/jcb.105.5.2279

Pedigo, S., and R.C. Williams Jr. 2002. Concentration dependence of variability in growth rates of microtubules. *Biophys. J.* 83:1809–1819. http://dx.doi.org/10.1016/S0006-3495(02)73946-5

Phirke, P., E. Efimenko, S. Mohan, J. Burghoorn, F. Crona, M.W. Bakhoum, M. Trieb, K. Schuske, E.M. Jorgensen, B.P. Piasecki, et al. 2011. Transcriptional profiling of *C. elegans* DAF-19 uncovers a ciliary base-associated protein and a CDK/CCRK/LF2p-related kinase required for intraflagellar transport. *Dev. Biol.* 357:235–247. http://dx.doi.org/10.1016/j.ydbio.2011.06.028

Preitner, N., J. Quan, D.W. Nowakowski, M.L. Hancock, J. Shi, J. Tcherkezian, T.L. Young-Pearse, and J.G. Flanagan. 2014. APC is an RNA-binding protein, and its interactome provides a link to neural development and microtubule assembly. *Cell*. 158:368–382. http://dx.doi.org/10.1016/j.cell.2014.05.042

Qian, H., M.P. Sheetz, and E.L. Elson. 1991. Single particle tracking. Analysis of diffusion and flow in two-dimensional systems. *Biophys. J.* 60:910–921. http://dx.doi.org/10.1016/S0006-3495(91)82125-7

Qin, H., D.R. Diener, S. Geimer, D.G. Cole, and J.L. Rosenbaum. 2004. Intraflagellar transport (IFT) cargo: IFT transports flagellar precursors to the tip and turnover products to the cell body. *J. Cell Biol.* 164:255–266. http://dx.doi.org/10.1083/jcb.200308132

Rasala, B.A., D.J. Barrera, J. Ng, T.M. Plucinak, J.N. Rosenberg, D.P. Weeks, G.A. Oyler, T.C. Peterson, F. Haerizadeh, and S.P. Mayfield. 2013. Expanding the spectral palette of fluorescent proteins for the green microalga *Chlamydomonas reinhardtii*. *Plant J.* 74:545–556. http://dx.doi.org/10.1111/tpj.12165

Rosenbaum, J.L., and G.B. Witman. 2002. Intraflagellar transport. *Nat. Rev. Mol. Cell Biol.* 3:813–825. http://dx.doi.org/10.1038/nrm952

Rosenbaum, J.L., J.E. Moulder, and D.L. Ringo. 1969. Flagellar elongation and shortening in *Chlamydomonas*. The use of cycloheximide and colchicine to study the synthesis and assembly of flagellar proteins. *J. Cell Biol.* 41:600–619. http://dx.doi.org/10.1083/jcb.41.2.600

Sbalzarini, I.F., and P. Koumoutsakos. 2005. Feature point tracking and trajectory analysis for video imaging in cell biology. *J. Struct. Biol.* 151:182–195. http://dx.doi.org/10.1016/j.jsb.2005.06.002

Shaner, N.C., G.G. Lambert, A. Chammas, Y. Ni, P.J. Cranfill, M.A. Baird, B.R. Sell, J.R. Allen, R.N. Day, M. Israelsson, et al. 2013. A bright monomeric green fluorescent protein derived from *Branchiostoma lanceolatum*. *Nat. Methods*. 10:407–409. http://dx.doi.org/10.1038/nmeth.2413

Sharma, N., Z.A. Kosan, J.E. Stallworth, N.F. Berbari, and B.K. Yoder. 2011. Soluble levels of cytosolic tubulin regulate ciliary length control. *Mol. Biol. Cell*. 22:806–816. http://dx.doi.org/10.1091/mbc.E10-03-0269

Shih, S.M., B.D. Engel, F. Kocabas, T. Bilyard, A. Gennerich, W.F. Marshall, and A. Yildiz. 2013. Intraflagellar transport drives flagellar surface motility. *eLife*. 2:e00744. http://dx.doi.org/10.7554/eLife.00744

Silflow, C.D., and J.L. Rosenbaum. 1981. Multiple α- and β-tubulin genes in *Chlamydomonas* and regulation of tubulin mRNA levels after deflagellation. *Cell*. 24:81–88. http://dx.doi.org/10.1016/0092-8674(81)90503-1

Srayko, M., A. Kaya, J. Stamford, and A.A. Hyman. 2005. Identification and characterization of factors required for microtubule growth and nucleation in the early *C. elegans* embryo. *Dev. Cell*. 9:223–236. http://dx.doi.org/10.1016/j.devcel.2005.07.003

Tam, L.W., N.F. Wilson, and P.A. Lefebvre. 2007. A CDK-related kinase regulates the length and assembly of flagella in *Chlamydomonas*. *J. Cell Biol.* 176:819–829. http://dx.doi.org/10.1083/jcb.200610022

Tam, L.W., P.T. Ranum, and P.A. Lefebvre. 2013. CDKL5 regulates flagellar length and localizes to the base of the flagella in *Chlamydomonas*. *Mol. Biol. Cell*. 24:588–600. http://dx.doi.org/10.1091/mbc.E12-10-0718

Tammachote, R., C.J. Hommerding, R.M. Sinders, C.A. Miller, P.G. Czarnecki, A.C. Leightner, J.L. Salisbury, C.J. Ward, V.E. Torres, V.H. Gattone II, and P.C. Harris. 2009. Ciliary and centrosomal defects associated with mutation and depletion of the Meckel syndrome genes MKS1 and MKS3. *Hum. Mol. Genet.* 18:3311–3323. http://dx.doi.org/10.1093/hmg/ddp272

Wang, L., T. Piao, M. Cao, T. Qin, L. Huang, H. Deng, T. Mao, and J. Pan. 2013. Flagellar regeneration requires cytoplasmic microtubule depolymerization and kinesin-13. *J. Cell Sci.* 126:1531–1540. http://dx.doi.org/10.1242/jcs.124255

Williams, C.L., C. Li, K. Kida, P.N. Inglis, S. Mohan, L. Semenec, N.J. Bialas, R.M. Stupay, N. Chen, O.E. Blacque, et al. 2011. MKS and NPHP modules cooperate to establish basal body/transition zone membrane associations and ciliary gate function during ciliogenesis. *J. Cell Biol.* 192:1023–1041. http://dx.doi.org/10.1083/jcb.201012116

Witman, G.B. 1975. The site of in vivo assembly of flagellar microtubules. *Ann. N. Y. Acad. Sci.* 253:178–191. http://dx.doi.org/10.1111/j.1749-6632.1975.tb19199.x

Witman, G.B. 1986. Isolation of *Chlamydomonas* flagella and flagellar axonemes. *Methods Enzymol.* 134:280–290. http://dx.doi.org/10.1016/0076-6879(86)34096-5

Wren, K.N., J.M. Craft, D. Tritschler, A. Schauer, D.K. Patel, E.F. Smith, M.E. Porter, P. Kner, and K.F. Lechtreck. 2013. A differential cargo-loading model of ciliary length regulation by IFT. *Curr. Biol.* 23:2463–2471. http://dx.doi.org/10.1016/j.cub.2013.10.044

Ye, F., D.K. Breslow, E.F. Koslover, A.J. Spakowitz, W.J. Nelson, and M.V. Nachury. 2013. Single molecule imaging reveals a major role for diffusion in the exploration of ciliary space by signaling receptors. *eLife*. 2:e00654. http://dx.doi.org/10.7554/eLife.00654